Doctor of Philosophy

Endothelial cells patterning by ultrasound standing wave for micro-vascular network generation in 3D engineered tissue

The Graduate School of the University of Ulsan

Department of Electrical, Electronic and Computer Engineering

Thi Huong Le

Endothelial cells patterning by ultrasound standing wave for micro-vascular network generation in 3D engineered tissue

Supervisor: Professor Koo, Kyo-in

A Dissertation

Submitted to the Graduate School of the University of Ulsan in

Partial Fulfillment of the Requirements for

the Degree of Doctor of Philosophy

by

Thi Huong Le

Department of Electrical, Electronic and Computer Engineering
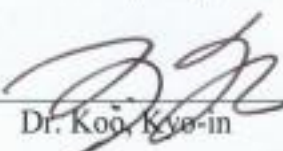
University of Ulsan, Korea

August 2024

Endothelial cells patterning by ultrasound standing wave for micro-vascular network generation in 3D engineered tissue

This certifies that the dissertation of Thi Huong Le is approved

Committee Chair: Dr. Back, Sung Hoon

Committee Member: Dr. Koo, Kyo-in

Committee Member: Dr. Chung, Su Wol

Committee Member: Dr. Kim, Dong

Committee Member: Dr. Kang, Hyun-Wook

Department of Electrical, Electronic and Computer Engineering

University of Ulsan, Korea

August 2024

Acknowledgments

First and foremost, I am extremely grateful to my supervisor, Prof. **Kyo-in Koo**, for his invaluable advice, support, and patience during my Ph.D. study. His immense knowledge and plentiful experience have encouraged me in all the time of my academic research and my daily life.

Besides my advisor, I would like to thank the rest of my dissertation committee: Prof. Sung Hoon Back, Prof. Su Wol Chung, Prof. Dong Kim, and Prof. Hyun Wook Kang for their encouragement, insightful comments that helped me to further improve my dissertation.

I highly appreciate and show my gratitude to Prof. Thomas Laurell (Lund University), Prof. Chaenyung Cha (UNIST) and his students, Mr. 이대영 (Kyungpook National University) for their co-working, service, and supporting during my Ph.D.

I would like to thank all members of the Medical Device Lab, University of Ulsan for working together, supporting each other and for all the fun we have had in the last six years.

Finally, I would like to express my gratitude to my parents and my big family. Without their tremendous understanding and encouragement, it would have been impossible for me to complete my study.

Thi Huong Le

Abstract

The development of functional and perfusable micro-vascular networks stands as a crucial role in the regeneration of tissues, particularly for the creation of large-scale, three-dimensional tissues. In recent years, the fabrication of micro-vascular networks has been a complicated multitask involving several different factors, such as time-consuming processes, cell survival, micro-diameter vasculature, and strict alignment requirements. In response to these challenges, an innovative approach that integrates multi-material extrusion with ultrasound standing wave forces to create a network structure of human umbilical vein endothelial cells within a composite matrix of calcium alginate and decellularized extracellular matrix was proposed. Through the improvement of cell-cell adhesion, the angiogenesis process, and perfusion tests using microparticles, FITC-dextran, and whole mouse blood, the functioning of the matured microvasculature networks was proven. Furthermore, animal experiments were conducted to assess the implantability and integration of the pre-formed vascular networks. The results showed that the pre-existing blood vessels of the host sprout towards the preformed vessels of the scaffold over time, and the micro-vessels inside the implanted scaffold matured from empty tubular structures to functional blood-carrying micro-vessels within two weeks. This approach was also employed for generating artificial liver scaffolds, which are the fundamental building blocks of liver tissue. Liver function and vascularization were both improved by the co-cultivation of two cell types. These findings highlight the potential of the proposed technique for the fabrication of large and complex tissue constructs with functional micro-vascular networks.

Contents

List of Figures

올산대학교
UNIVERSITY OF ULSAN

울산대학교
UNIVERSITY OF ULSAN

울산대학교
UNIVERSITY OF ULSAN

List of Abbreviations

No.	Short name	Full name
1	EC	Endothelial cell
2	ECM	Extracellular matrix
3	3D	Three-dimensional
5	PAD	Peripheral artery disease
6	GelMA	Gelatine methacryloyl
7	PEGOA	Poly(ethylene glycol) acrylate
8	UV	Ultraviolet
9	dECM	Decellularized extracellular matrix
10	L-dECM	Liver decellularized extracellular matrix
11	HUVEC	Human umbilical vein endothelial cell
12	RFP-HUVEC	Red fluorescent protein Expressing Human Umbilical Vein Endothelial Cell
13	NIH/3T3	Mouse fibroblast
14	PDMS	Polydimethylsiloxane
15	CaCl$_2$	Calcium chloride
16	NaCl	Sodium chloride
17	PBS	Phosphate buffered saline
18	NaOH	Sodium hydroxide
19	DMEM	Dulbecco's Modified Eagle Medium
20	SEM	Scanning electron microscopy
21	DMSO	Dimethyl sulfoxide
22	FBS	Fetal bovine serum
23	RT	Room temperature
24	ID	Inner diameter
25	OD	Outer diameter

울산대학교
UNIVERSITY OF ULSAN

26	GF	Growth factor
27	EDTA	Ethylenediaminetetraacetic acid
28	FITC-Dextran	Fluorescein isothiocyanate–dextran
29	HE	Hematoxylin and eosin
30	BSA	Bovine serum albumin

Chapter 1: Introduction

1.1 Vascularization in tissue engineering

In recent years, a large number of patients have died because of a significant increase in the gap between the number of patients waiting for organ transplantation and the available donor organs [1]. To tackle this challenge, recent advancements in bio-fabrication techniques have demonstrated considerable potential by amalgamating live cells, biocompatible materials, and chemicals. However, the failure to develop a dense microvascular network inside the artificial organs makes it difficult to fabricate full-sized, sustainable, and functional three-dimensional (3D) organs [2]. The vascular network is critical for the distribution of nutrients, oxygen, and the removal of metabolic waste products to sustain tissue metabolism and growth; it is the complex network of arteries, veins, and capillaries found in real organs [3-5]. Without this vital network, artificial organs risk succumbing to tissue necrosis and ischemic diseases, rendering them nonviable for transplantation. The greatest distance between a vessel and cells is limited to less than 200 μm, which is a key threshold determined by the principles of diffusion limitation [6-8]. Hence, rapid revascularization and the generation of a functional, dense microvascular network are crucial for the successful engineering of large and complex tissue constructs.

Capillaries are the smallest blood vessels in the vascular network, and they link the arterioles with the venules. Its features include fenestration at the junctions between endothelial cells, which varies in size depending on the vascularized organ, and a mean diameter of about 10 μm [9, 10]. Despite their tiny appearance, these micro-vascular structures play indispensable roles in vital physiological processes such as circulation, gaseous exchange, nutrient transfer, and various other components which are exchanged between the bloodstream and surrounding cells or tissues. The structure of a capillary wall is characterized by an endothelial layer enveloped by a basement membrane,

2

occasionally interspersed with smooth muscle fibers. In a large capillary, the lumen (inner space) is lined by multiple endothelial cells that border and align with each other. In contrast, a small capillary typically has a single layer of endothelial cells that wraps around to form a continuous tube, with the cell layer in direct contact with itself. The level of "leakiness" in capillaries may be classified into three main categories: sinusoid, fenestrated, and continuous capillaries (Figure 1). Nearly all vascularized tissues contain the continuous capillary, which is the most common type of capillary [11-13].
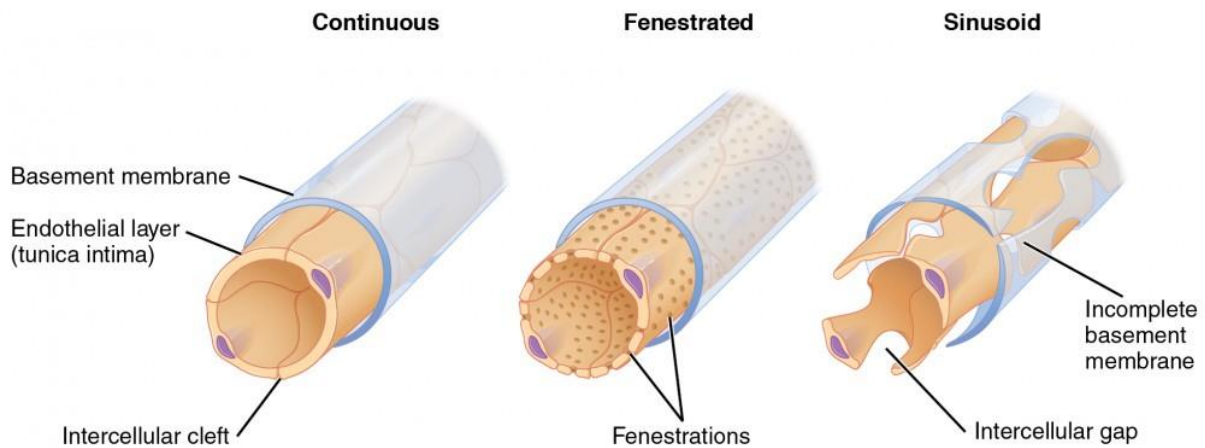
Figure 1. The structure of three types of capillary [11]

There have been many attempts to embed vascular networks into three-dimensional (3D) artificial tissue structures; the use of 3D bioprinting techniques is one of the most well-known approaches. This approach uses specialized 3D bioprinters to create vascular structure by combining cells, biomaterials, and biologically active ingredients.

Endothelial cells (EC) serve as a crucial cornerstone in the process of revascularization. These cells, which line the inner walls of blood vessels, are instrumental in angiogenesis—the physiological mechanism underlying the formation of new blood vessels [14-16]. The formation of a vascular network can occur through two primary mechanisms: vasculogenesis and angiogenesis.

Vasculogenesis involves the *de novo* creation of blood vessels, while angiogenesis extends existing vascular structures by fostering the growth of new vessels from pre-existing ones [17-20].

Biomaterials can be produced synthetically or from natural sources and utilized to replace tissue, either completely or partially. They must be biocompatible and biodegradable or avoid the activation of immune reaction and bioactive to stimulate tissue response [21, 22]. Natural materials such as chitosan, gelatin, collagen, cellulose, alginates, extracellular matrix (ECM), etc., are more suggested than synthetic materials (polylactide-co-glycolide (PLGA), polycaprolactone (PCL), polylactic acid (PLA), fibronectin, polyurethane, etc.) because they have good biocompatibility, excellent biodegradability, and minimal toxicity [23-25]. Among them, ECM – which is an isolated extracellular matrix from native tissue – has been used widely in tissue engineering due to its high porosity and specific peptide sequences. It can supply both physical and mechanical microenvironments for cells to survive and proliferate during the vascular network formation process [26-29].

1.2 Ultrasound standing wave

Ultrasound standing wave (USW) can be employed to manipulate particles within fluids. It has been reported as a simple, fast, and non-invasive way for rapid patterning of microparticles and cells within 3D hydrogels. Acoustic waves are the transmission of perturbation through a medium. It travels lengthwise across the medium at the speed of sound, with the pressure vibration's direction matching the wave's propagation direction [30, 31]. USW can be created by the superposition of the incident and reflected waves when ultrasonic waves are transmitted through a fluid within a chamber and the chamber walls function as reflectors. The regions where the superposition is destructive are called nodes whereas the regions where the superposition is

울산대학교
UNIVERSITY OF ULSAN

constructive are called antinodes [32-34]. USW induces an acoustic radiation force, F^{rad}. This force acts to relocate particles and droplets towards either the node or antinode of the standing wave (Figure 2) depending on the sign of the acoustic contrast factor ϕ. This factor, determined by the density and compressibility of the particles as well as the properties of the surrounding medium, dictates the direction of movement within the acoustic field [35, 36].
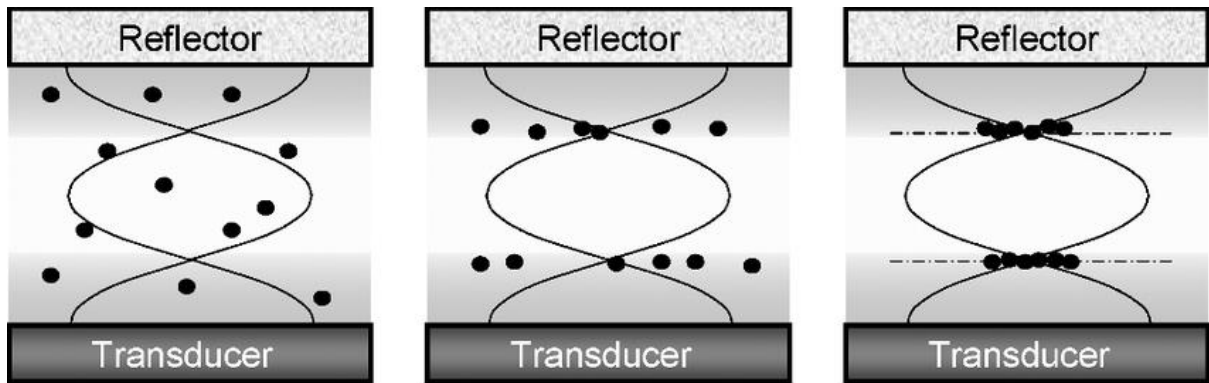
Figure 2. Particle movement inside an ultrasonic standing wave (USW) [36]

The radiation force is derived as follows, when considering a one-dimensional standing wave:

$$F^{rad} = 4\pi k\varepsilon\alpha^3 \; \phi(\beta,\rho) \sin(2kx) \qquad (1)$$

The term of the acoustic contrast factor $\phi\,(\beta,\rho)$, is given by:

$$\phi\,(\beta,\rho) = \frac{\frac{2}{3}(\rho_p - \rho_f)}{2\rho_p + \rho_f} - \frac{\beta_p}{3\beta_f} \qquad (2)$$

where α is radius of a spherical particle at a position x within a one-dimensional standing wave of acoustic energy density ε. β and ρ are the compressibility and the mass density of the fluid (f) and the particle (p), respectively. The compressibility connected with the speed of sound, c by $\beta = \frac{1}{\rho c^2}$. The wave number, $k = 2\pi/\lambda$ where λ is the wavelength [36, 37].

1.3 Objectives

In this dissertation, an ultrasound standing wave was used for patterning endothelial cells inside the dECM-based hydrogel. The combination of the continuous extrusion method and ultrasound cell manipulation resulted in cells arranged as branched structures. Culturing the branching-structured scaffold with alginate lyase enabled the entrapped HUVECs to form a microvasculature network structure. The functional properties including cell-cell adhesion, angiogenesis, and perfusability with microparticles, FITC-dextran, and whole mouse blood were observed. Furthermore, the implantability was also demonstrated.

1.4 Dissertation arrangements

The dissertation's structure will be organized into four chapters as below:

Chapter 1 describes the literature introduction to vascularization in three-dimensional engineered tissue. After that, a review of the principle of ultrasound standing wave. The final parts report the targets and dissertation organization.

Chapter 2 and **Chapter 3** present the pattering of endothelial cells for 3D micro-vascular network formation by using ultrasound standing wave.

Chapter 4 summarizes the obtained achievements and limitations in this dissertation and gives out some feasible solutions and perspectives.

Chapter 2: Endothelial cells patterning by ultrasound standing wave for micro-vascular network generation in 3D engineered tissue

2.1 Background

In the native tissue structure, the microvascular networks are organized as a hierarchical distribution of progressive branching vessels, which is how blood is distributed throughout the tissues [38]. Therefore, branching is an essential procedure that is vital to the structure and operation of the vessel network The vascular networks must fulfill certain conditions in order for the designed tissue to survive over time and operate properly; (1) a 3D dense network to surpass the 200 µm diffusion limit of oxygen and nutrients, (2) branching connections to cover the maximum tissue volume, (3) functions of angiogenesis and perfusion, (4) implantability to target host [39-42].

Pre-vascularized tissue constructions have been the subject of investigation for several research groups in the past few years. Despite the remarkable outcomes, a few limitations still exist. In bio-printing, techniques the alignment of cell-laden layers is strictly required [43, 44] or only individual channels without any branching were made [45, 46]. An alternative strategy uses the drop-on-demand technique and is based on the ability of ECs to self-assemble [47]. Droplets containing ECs are printed onto a gel substrate. This approach does not facilitate the generation of smaller vessels than the printed droplet and is time-consuming to formulate the cell-spheroid.

USW has the potential for various applications in bio-fabrication and biomaterial fields such as vascular morphogenesis [34], myotubes organization [48], separation [49-51], and enrichment [52-54]. Acoustic standing waves generate regions of pressure nodes and pressure anti-nodes and based on the cell's size, density, and compressibility; they can be acoustically moved toward the pressure nodes [31, 32].

In this chapter, the combination of a multi-material extrusion technique and USW to generate ECs in a network structure within a mixture of calcium

alginate and decellularized extracellular matrix (dECM) from pig was investigated. Culturing the branching-structured scaffold with alginate lyase enabled the entrapped ECs to form a microvasculature network structure. Functionality and implantability of the matured microvasculature network were demonstrated. It served as a testament to the ingenuity of scientific methodology, showcasing the potential for engineered constructs to mimic and even enhance biological processes.

2.2 Theory and concept

The method generated acoustic nodes inside the pre-hydrogel material to obtain a branched EC structure and extruded three hydrogel layers for HUVECs' migration and maturing to vessels, as shown in Figure 3. The USW at frequency 2 MHz in two types of square glass capillaries (400 µm and 800 µm) could generate a transition from one focused cell stream to four cell streams of HUVECs and vice versa.

(a) HUVEC scaffold fabrication   (b) HUVEC scaffold culturing   (c) *In vivo* study

□ Outer layer: Alginate ■ Inner layer: dECM+Alg ▨ HUVECs ■ dECM ◯ Migrated HUVECs
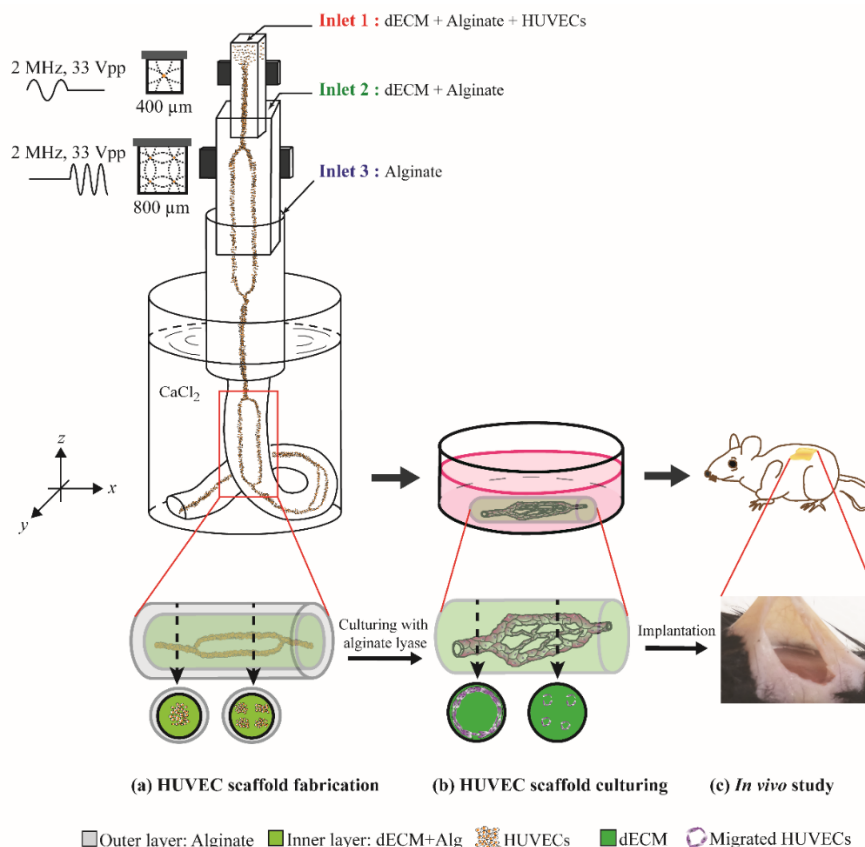
Figure 3. Schematic of the HUVECs patterning in hydrogel using ultrasound and the following in vivo study. (a) The HUVEC scaffold fabrication using ultrasound standing waves. (b) The HUVEC scaffold culturing with alginate lyase. (c) The implantation of the matured HUVEC scaffold.

When applying 2 MHz ultrasound in a 400 µm square-shaped glass capillary, a half-wavelength standing wave was formed in both the x- and the y-direction with the pressure node in the channel center (Figure 4(a)), which was described and demonstrated in our previous report [37]. When the capillary was doubled to 800 µm, the square capillary supported a full wavelength resonance in both the x- and y-directions, and hence four pressure nodes were generated in the capillary cross-section, located $\lambda/4$ from the channel side walls (Figure 4(b)).
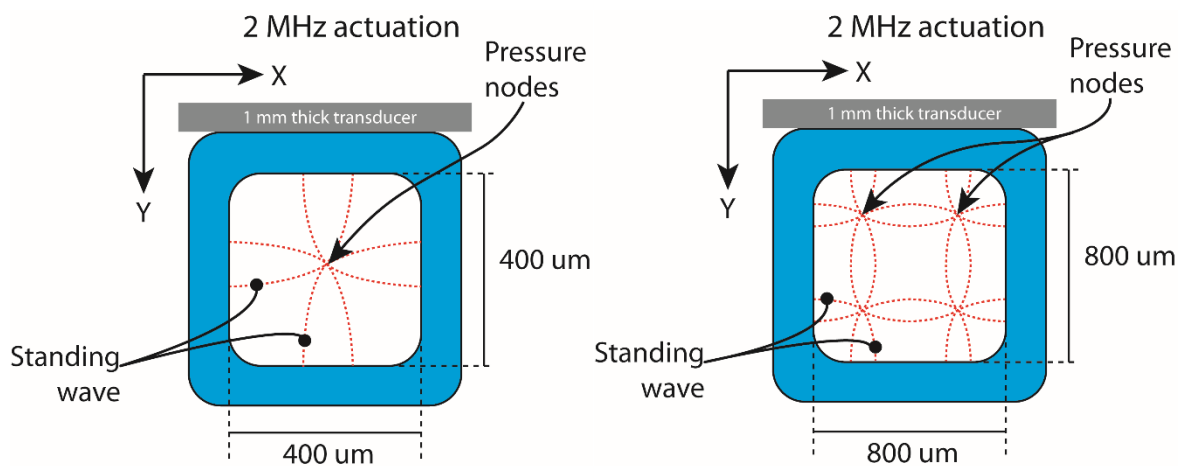
Figure 4. Schematic of the standing wave pattern in the capillary cross-section when actuated (a) at 2 MHz in 400 µm square-shaped glass capillary, yielding a single pressure node in the center for microparticle or cell focusing, and (b) at 2 MHz in the 800 µm square-shaped glass capillary, providing four pressure nodes, one in each cross-section quadrant for microparticle or cell focusing. The transducer dimensions are not to scale in the drawing.

Using red polystyrene microparticles, Figure 5 demonstrates the principle of focusing particles or cells in the acoustic standing wave field. The acoustic

radiation force of the 2 MHz actuation in the 400 µm square capillary focused the microparticles into one stream at the center of the capillary (Figure 5(b)). In the case of the 800 µm square capillary, four parallel lines of microparticles were generated in the sodium alginate. Due to their alignment at the regular quadrilateral points, some of the lines were obscured by the others when viewed under a two-dimensional microscope, as shown in Figure 5(c). Based on this concept, alternating on and off 2 MHz ultrasound in the 400 µm and 800 µm square capillary patterned one line and four lines in a continuous linear structure, resulting in the branched and merged structure (Figures 5(d)–(f)), and with ECs as shown in Figure 3.
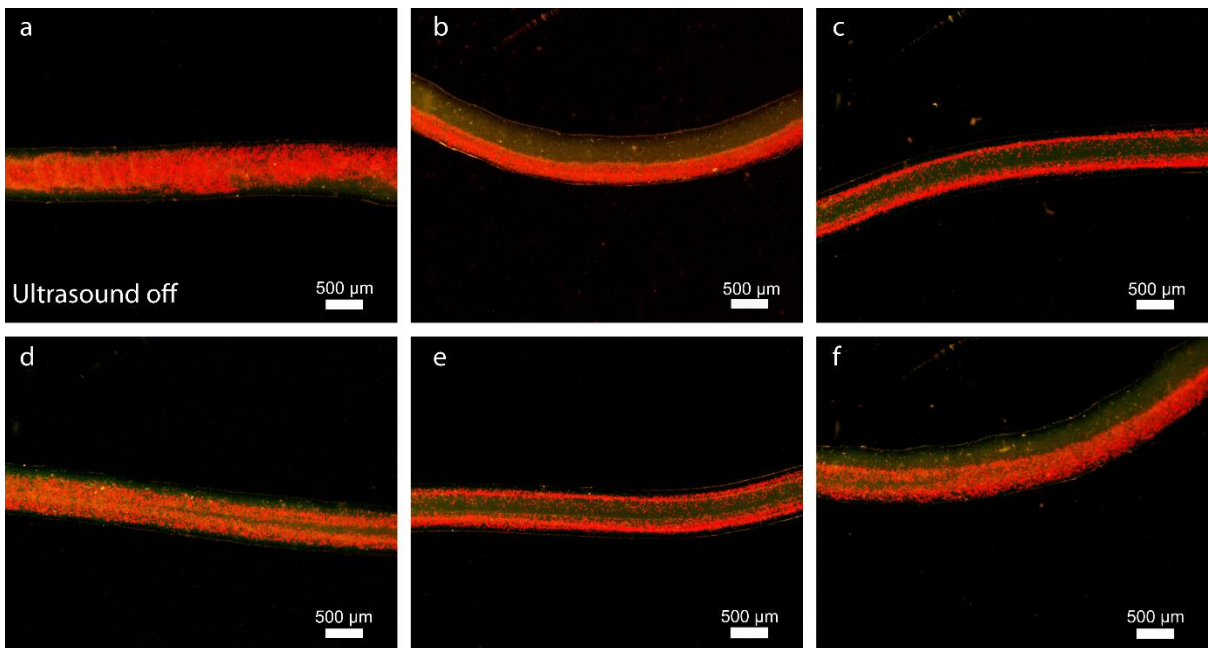
Figure 5. The polystyrene microparticle (red) in the mixture of the sodium alginate and the dECM. (a) The microparticles unexposed to ultrasound. (b) The aligned microparticles as one stream by the ultrasound. (c) The aligned microparticles as four streams by ultrasound. (d) The patterned microparticles in transition from one stream to four streams. (e) The aligned microparticles as four streams. (f) The patterned microparticles in transition from four streams to one stream. The top view obscures the two underlying particle lines.

11

2.3 Materials and methods

2.3.1 Hydrogel preparation

Three hundred fifty milligram dECM powder and 200 mg pepsin (Sigma-Aldrich, St. Louis, MO, U.S.A.) dissolved in 1 mL acetic acid (Sigma-Aldrich, St. Louis, MO, U.S.A.) and DI water to make 35 mg/mL concentration dECM of 100 mL total volume solution. The solution was stirred for 72 – 96 hours at room temperature (RT). After that, the dissolved dECM was centrifuged at 3000 rpm for 15 min. The supernatant was carefully transferred into other conical tubes, and then the remaining non-dissolved components were discarded. The tubes containing dissolved dECM was kept in storage at 2 – 8 °C.

For dECM neutralization and dilution, the 35 mg/mL dECM was mixed with 10 M and 1M NaOH (Sigma-Aldrich, St. Louis, MO, U.S.A.) and 10X PBS (10% of the total volume) to adjust pH range from 7.2 to 7.5 and 25 mg/mL dECM concentration (Figure 6). Final hydrogel for acoustic pattering was a mixture of sodium alginate (MERCK, Madison, NJ, U.S.A.) (0.5% w/v) and dECM (25 mg/mL) at ratio 1:9. All these steps were processed on ice to avoid gelation.
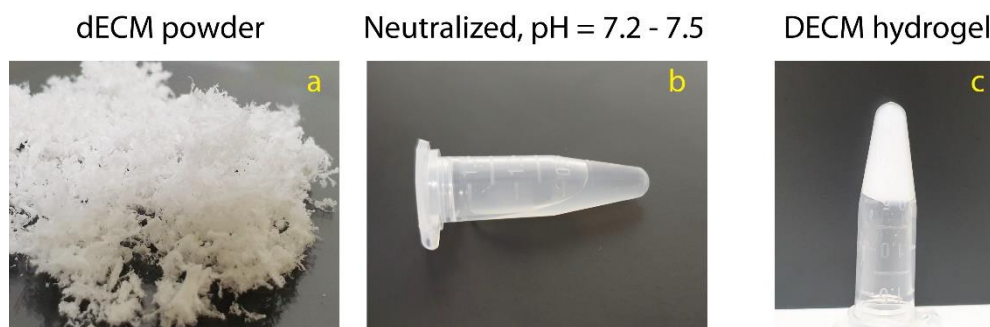
Figure 6. The dECM hydrogel preparation. (a) The dECM powder. (b) The dECM powder is dissolved and neutralized to 7.2 – 7.5 pH. (c) The neutralized dECM was gellated in 37 ˚C for 10 minutes.

2.3.2 Cell culture

Human umbilical vein endothelial cells (HUVEC) were purchased from ATCC (PCS-100-010, cryopreserved, ATCC, U.S.A.) and RFP Expressing Human Umbilical Vein Endothelial Cells (RFP-HUVEC) were purchased from Angio-Proteome (cAP-0001RFP, Angio-Proteome, U.S.A). Cell culture medium included EGMt-2 Endothelial Cell Growth Medium-2 Bullet Kit (Lonza, Basel, Switzerland) and 1% penicillin/streptomycin (Sigma-Aldrich, St. Louis, MO, U.S.A.). The HUVECs were seeded on cell culture polystyrene dishes and incubated at 37 °C and 5% CO_2. The cells within passages 6 − 10 were used in experiments.

2.3.3 Multi-line patterning using ultrasound standing wave

As shown in Figure 3, 1 mm thick ultrasound transducers (MEGITT A/S, Kvistgaard, Denmark) glued to a 400 µm and an 800 µm square-shaped glass capillaries (VitroCom, NJ, U.S.A.) respectively. The device has three inlets. The mixture of sodium alginate and dECM was mixed with 60 µL of 10-micrometer (diameter) polystyrene microparticles (MERCK, Madison, NJ, U.S.A.) and was pumped into the inlet 1. The same ratio of dECM and alginate without any microparticles was supplied into inlet 2. Sodium alginate (1% w/v) was only injected into the inlet 3. The flow rate for the inlet 1 is 30 µL/min, the inlet 2 is 30 µL/min and the inlet 3 is 150 µL/min. For cell experiments, 100 µL of HUVECs used instead of the microparticles. The outlet was immersed into a beaker of 300 mM $CaCl_2$ (MERCK, Madison, NJ, U.S.A.) for cross-linking. After that, the scaffold was incubated at 37°C for at least ten minutes to enable dECM gelation.

2.3.4 Microvascular network formation

The extruded cell-laden scaffolds were cultured in conventional HUVEC media described previously for one day at 37 °C and 5% CO_2 to maintain the extruded three-layered structures intact. After one day of the conventional culturing, alginate lyase enzyme (MERCK, Madison, NJ, U.S.A.) was added into the conventional HUVEC media at a final concentration of 0.1 unit/mL to dissolve calcium alginate ingredients in the layered scaffolds for HUVEC migration. The alginate-degrading media was replaced every day.

2.3.5 Mice

The C57BL/6 mice (3-8 weeks old, 15–35 g) were purchased from KOATECH (Pyeongtaek, Republic of Korea). The mice were kept in a facility with 60% humidity at 24 °C, a 12-hour light/dark cycle, and free access to drinks and food. Animal studies were performed in line with the principles and guidelines of laboratory animal care and ethics, with permission from the University of Ulsan's Institutional Animal Care and Use Committee (GIG-22-030 and GIG-22-040, University of Ulsan, Ulsan, Republic of Korea). The experiment was conducted three times using a total of nine mice.

2.5.6 Whole blood collection and labelling (cell tracker)

Mouse whole blood was collected using tail vein collection technique [55]. One milliliter of whole blood was collected from a 20 – 30 g mouse. The gathered whole blood was mixed with heparin (Sigma, U.S.A.) at 30 USP units/mL as the final concentration. The heparinated whole blood was incubated with a cytoplasmic probe and 10 µM Cell Tracker™ Green BODIPY™ dyes (C2102, Thermo Scientific, U.S.A.) for 35 minutes following manufacturer's instructions before perfusing.

2.5.7 Perfusablility assay

A lab-made connector (Fig. 7a) holds the matured scaffold using additional calcium alginate hydrogel. To secure pumping, a glass capillary (ID: 50 µm, OD: 80 µm, VitroCom, NJ, U.S.A.), the red one in Fig. 7a, was inserted into a vessel of the matured scaffold. The big glass tube (the black one) was made of a capillilary (1.15 mm inner diameter and 1.55 mm outer diameter) (Marienfeld, Germany). It was restricted with a PC-10 puller (Narishige International, U.S.A.). Solutions such as 5 µm fluorescent microparticles, whole blood of mouse, or fluorescein isothiocyanate dextran (FITC-dextran) 70 kDa was injected at a constant flow of 15 µL/min. After perfusing for 5 minutes, the HUVEC scaffold was washed with 1X PBS buffer for microscope observation.
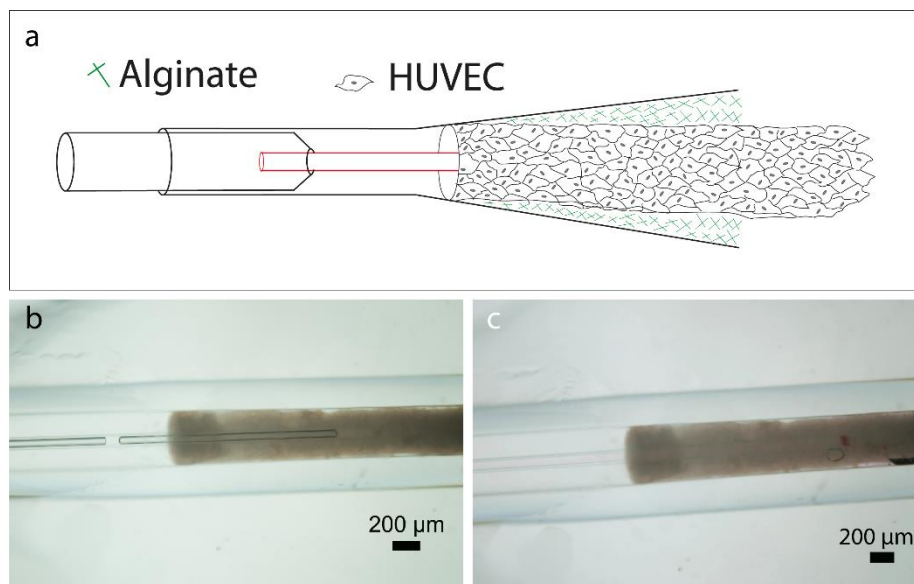
Figure 7. (a) The illustration about the perfusability experiment. The connecting area (b) before and (c) after pumping the food dye. The HUVEC scaffold was fixed by additional alginate at to the lab-made connector and then a glass capillary (the red one tube in (a) secured connection from the left guide glass tube (the black tapered one in (a) to the one-line region of the HUVEC scaffold.

2.3.8 Implant surgery

A mouse (6-8 weeks and 20-30 g) was anesthetized using 2,2,2-Tribromoethanol (~240 mg/kg) (Sigma-Aldrich, St. Louis, MO, U.S.A.). The hair was removed by Nair gel (Church& Dwight UK Ltd., Kent, U.K.) and povidone-iodine 10% (Forson, Chungcheongnam, Republic ok Korea) applied for disinfection before surgery. The skin on the back of the mouse opened about ~ 30 mm in length and ~ 20 mm in wide using scissors and fine forceps. The matured scaffold (~ 2 cm in length) placed under the skin. After that, the open skin was closed using black silk suture 4-0 (Ailee, Busan, Republic of Korea). The implanted mouse was kept warm for 3-4 hours to recover. The mouse recovered separately and its inflammation after the surgery was monitored visually during the recovery time. For harvesting the implanted scaffold, the operated mouse was anesthetized one more time on day 3, 7 and 14. After harvesting, the anesthetized mouse was performed cervical dislocation until respiration stopped for euthanasia. All surgical instruments were autoclaved before the experiments.

2.3.9 Immunofluorescent staining

The HUVECs scaffold were fixed in 4% paraformaldehyde (Sigma-Aldrich, St. Louis, MO, U.S.A.) for 25 minutes at RT, permeabilized with 0.5% Triton-X100 (Sigma-Aldrich, St. Louis, MO, U.S.A.) for 5 minutes, and then treated with 5% bovine serum albumin (BSA) (Sigma-Aldrich, St. Louis, MO, U.S.A.) as blocking solution for 20 min at RT. The primary antibody CD31 (1:50) (Thermo Scientific, Waltham, Massachusetts, U.S.A.), ZO-1 (1:100) (Thermo Scientific, Waltham, Massachusetts, U.S.A.), VE-cadherin (1:100) was incubated with the treated scaffolds at 4 ℃ overnight. Subsequently, the scaffolds were incubated with a goat anti-mouse IgG (H + L) highly cross adsorbed secondary antibody, Alexa Fluor plus 488 (1:1000) (Thermo Scientific, Waltham, Massachusetts, U.S.A.) for 120 minutes at RT. The nuclei were

stained with 4′,6-diamidino2-phenylindole (DAPI) (NucBlue® Live ReadyProbes™ Reagent, Thermo Scientific, Waltham, Massachusetts, U.S.A.) for 15 minutes before imaging. The scaffolds were washed with 1X PBS buffer (3 time/5 min) between steps.

2.3.10 Imaging and Statistical analyses

The cell-stained scaffolds were observed with an IX53 inverted fluorescent microscope (Olympus, Tokyo, Japan), and pictures were taken with CellSens software (Olympus, Tokyo, Japan). A laser scanning confocal microscope (FLUOVIEW FV1200, Olympus, Tokyo, Japan) was used for three-dimensional imaging. All data were shown as the mean ± standard deviation (SD). ImageJ (NIH, Washington, U.S.A.) was used for image preparation and analysis.

Cell viability was determined using a ratio calculation between the mean grey value (gv) of 2 color channels (green for live cells and red for dead cells) on a black background. The grey values were obtained from 4X confocal images, which were split into 2 separate color channels using ImageJ. The calculation was carried out according to the following equation [56]:

$$Cell\ viability = \frac{green\ gv}{green\ gv\ +\ red\ gv} \times 100\%$$

2.4 Results and discussion

2.4.1 Mixture of calcium alginate and dECM as a scaffold material

Via ionic crosslinking with calcium (Ca^{2+}) sodium alginate can form calcium alginate hydrogel rapidly [57, 58]. To preserve the branched cell structure inside the hydrogel, the pre-hydrogel material should be gellated as soon as possible right after the acoustic patterning. However, as shown in our

earlier study the animal cells could not migrate and proliferate well in calcium alginate because it cannot synthesize endogenous alginase for alginate degradation [37, 59].

Therefore, a mixture of dECM from pig (Fig. 6) and sodium alginate at 9:1 of ratio was utilized as pre-hydrogel in this study. The dECM hydrogel has both characteristics of holding cells as scaffolds and working as functional extracellular matrix. It contains functional components of native tissue including collagen fibers, glycosaminoglycans (GAGs), growth factors, and more. Therefore, it provides an excellent extracellular microenvironment for cells adhesion, differentiation, proliferation, and functional expression [60-62].

Fig. 8 a – c shows the microstructure of dECM, calcium alginate, the mixture of calcium alginate and dECM, the mixture of the calcium alginate and the dECM after alginate lyase, respectively. The dECM presented more fibrous structure and higher porosity compared to calcium alginate only. These characteristics provided a better microenvironment for cell adhesion and migration. In the mixture of dECM and calcium alginate, fiber diameter and pore size increased. This change might be due to the cross-liking reaction between $CaCl_2$ and dECM molecules [63].

The experimental outcomes further reveal that calcium alginate scaffold exhibits the most favorable mechanical properties, marked by the highest breaking force results, but the lowest diffusibility. On the other hand, the dECM scaffold showed the best diffusibility, it presented challenges in terms of handling. Meanwhile, the scaffold with mixture of calcium alginate and dECM can be easy to handle while maintaining adequate diffusibility. After removing the calcium alginate from the mixture scaffold, it showed the fibrous structure but also had difficulties when handling like dECM scaffold (Fig. 8 d – g).
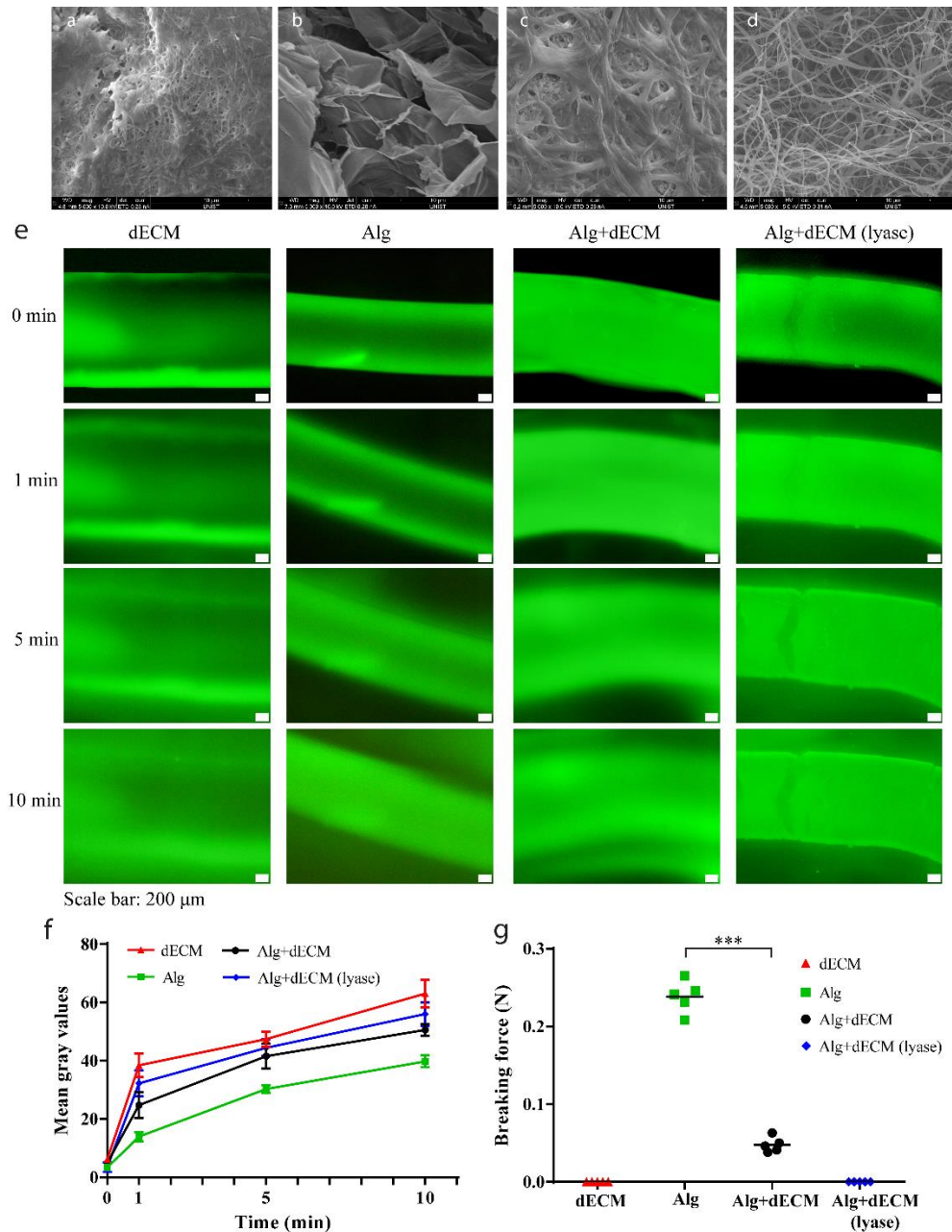
Figure 8. The scanning electron microscopy (SEM) images of (a) the dECM hydrogel, (b) the calcium alginate hydrogel, and (c) the mixture of the calcium alginate and the dECM, (d) the mixture of the calcium alginate and the dECM after alginate lyase. (e) The time-lapse fluorescent images of FITC-Dextran diffusion of the dECM, the calcium alginate, and the mixture of the calcium alginate and dECM, the lysed-calcium alginate hydrogel scaffold from 0 min to 10 min. (f) The fluorescent intensity was analyzed with respect to the time (n=3). (g) The breaking force of the hydrogel scaffold (*** $p < 0.001$, n = 5).

2.4.2 Branched structure with ECs

For three-dimensional vascular network formation, HUVECs were patterned alternating in a single line and in four lines. From the cross-section image (Fig. 9a and b), four groups of manipulated cells were distinguishable corresponding to the acoustic nodal positions. The extraction of beam intensity from cross-sectional confocal images also showed that particles were concentrated at specific locations corresponding to the acoustic nodes (Fig. 9c).
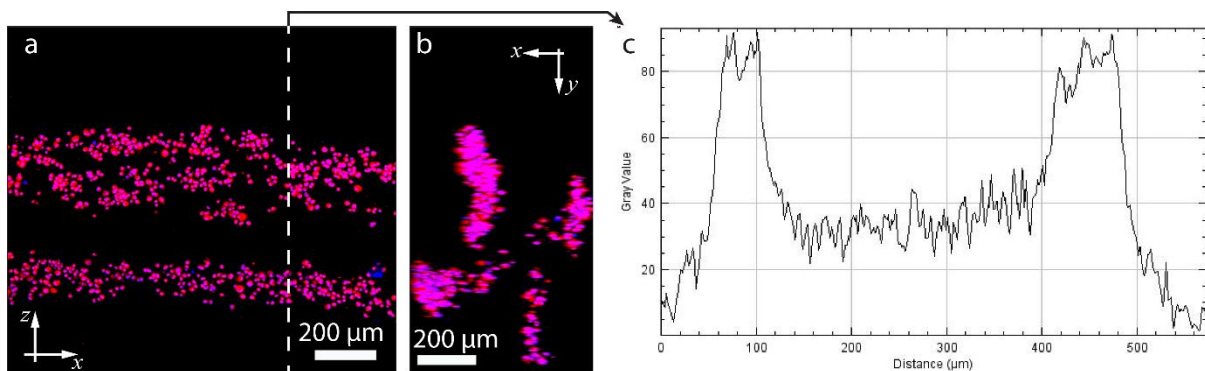
Figure 9. (a) Top view of the RFP-HUVECs aligned as four lines. (b) Confocal cross-section (z-stack) of the of the four focused cell regions. The red is RFP-HUVEC. The blue is DAPI. (c) Spatial distribution of the fluorescence intensity in (a).

It is well known that cell concentration and acoustic power significantly influenced the patterned structures [64, 65]. In our hydrogel mixture, 1×10^6, 5×10^6 and 8×10^6 cells/mL of HUVECs were patterned using an actuation voltage of 20 VPP and 33 VPP, as shown in Fig. 10. As the cell concentration and the acoustic power increased, the width of the grouped cells and inter-distance between the groups also increased.

20
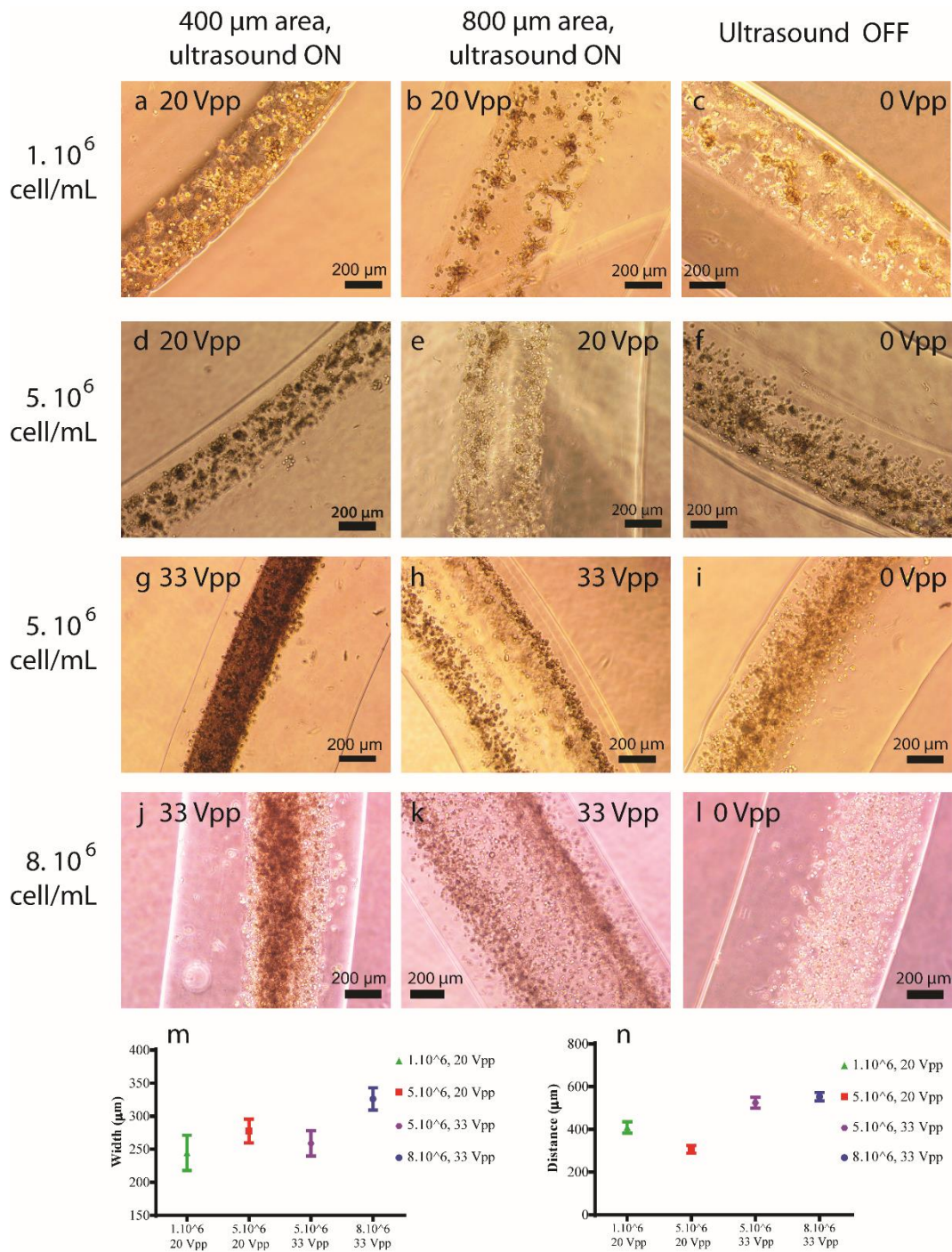
Figure 10. The relationship between the ultrasonic power and the HUVEC density. (a- c) The bright-field microscope images of (a - c) 1×10^6 cells/mL, (d - f) 5×10^6 cells/mL, (g - i) 5×10^6 cells/mL, and (j - l) 8×10^6 cell/mL. (m) The width changes of the one line region. (n) The distance change between the aligned HUVECs in the four lines region.

Temperature measurement on the backside of the transducers after ten-minute operating at 33 VPP saturated under 40 ℃ (Fig. 11), which is the upper limit temperature condition of the hydrogel for the cell viability [66]. Live and dead cell fluorescent images of the 33 VPP scaffold were not easy to discriminate from those of the 20 VPP scaffold (Fig. 12). Cell viability of scaffolds made at both actuation voltages was found to be about 90% (Fig. 13).
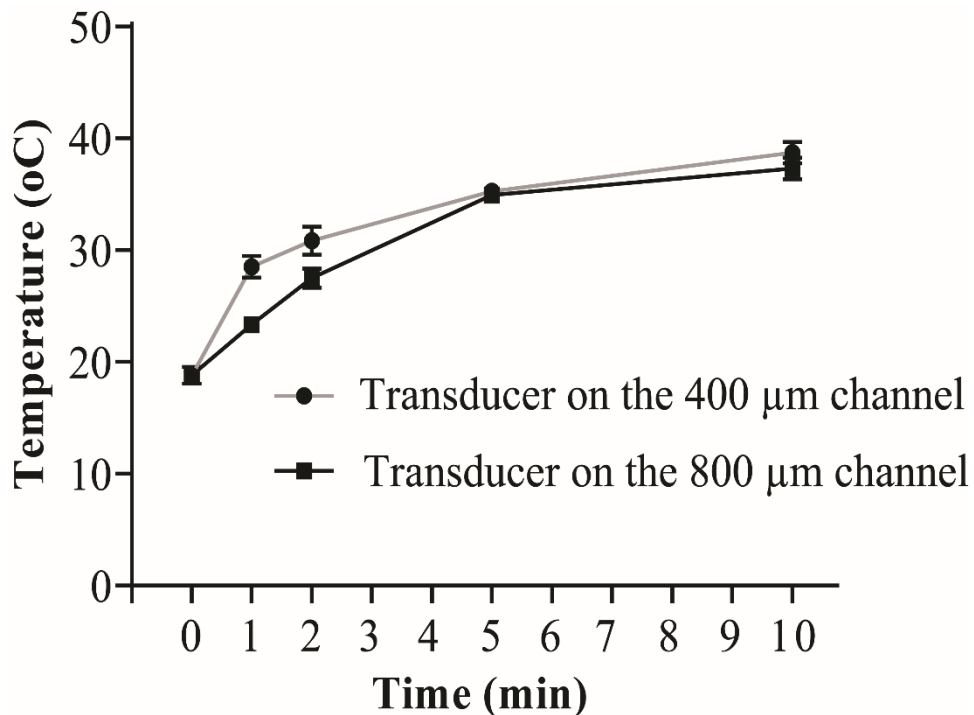
Figure 11. The temperature of the transducers with respect to time at 33 Vpp and 2 MHz.
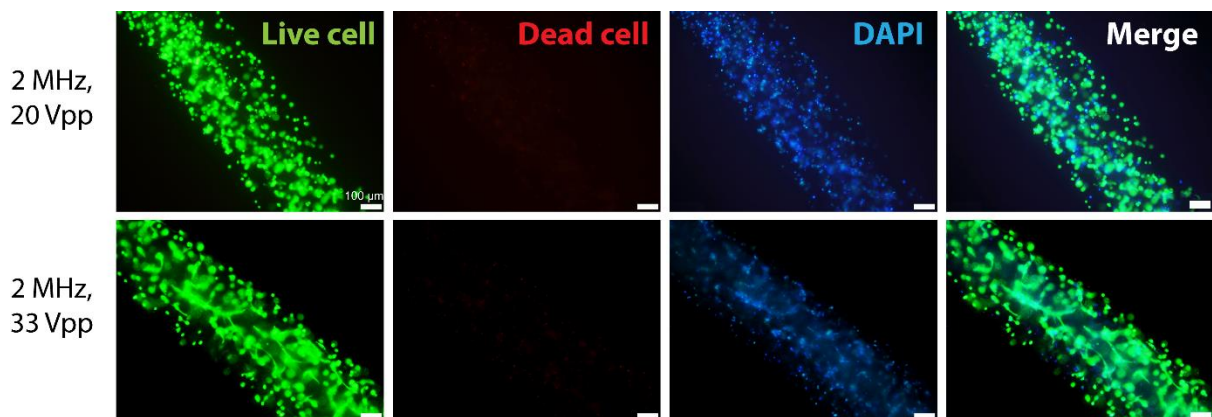
Figure 12. The live and dead fluorescent images of the HUVECs in the scaffold 12 hours after exposed 2 MHz ultrasound (20 Vpp and 33 Vpp). The green is a live cell. The red is a dead cell. The blue is DAPI.
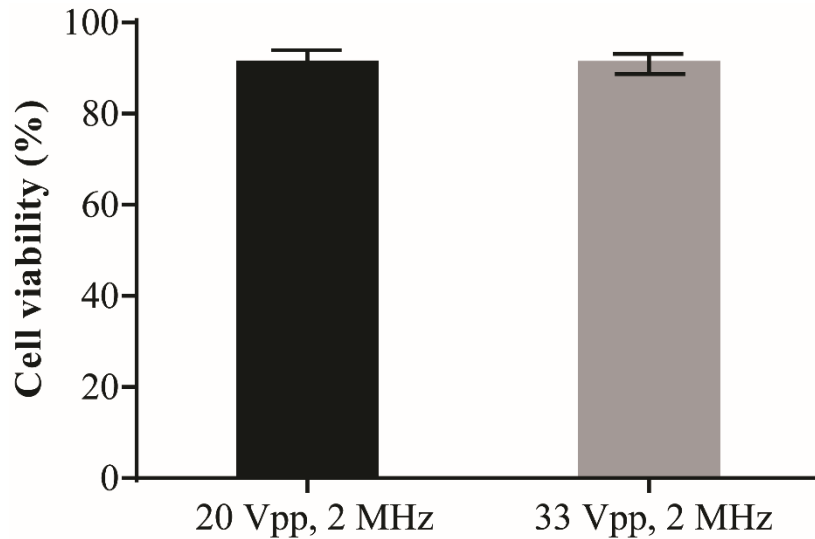
Figure 13. The cell viability with respect to the transducer-driving voltages (20 Vpp and 33 Vpp). The repetition number is 5.

2.4.3. Enhanced HUVEC proliferation by alginate enzyme

It is known that animal cells have no receptors to recognize alginate which is required for signaling production between cells and external matrix interaction [67, 68]. This results in limited animal cell proliferation in an alginate scaffold. Therefore, in this manuscript, HUVECs scaffolds were cultured together with alginate lyase which degrades alginate through breaking glycosidic bond [69]. The microstructure of the mixture of dECM and calcium alginate scaffold after the degradation of calcium alginate showed the fibrous structure which can serve as a supportive extracellular matrix for cell growth (Fig. 8d).

The HUVEC scaffold cultured with alginate lyase exhibited more cell-cell adhesion and better lumen formation than the non-lyase scaffold in the one-

line region (Fig. 14 e and f). In the four-line region, the HUVEC scaffold with lyase appear to show a more lumen like formation than the non-lyase scaffold. (Fig. 6 g and h). This trend is presented in the cell-occupying ratio graph and the cell perimeter graph (Fig. 14 i – j and Fig. 15) as well. The cell-occupancy of the lyase-culturing scaffold increased from $60.4 \pm 6.8\%$ at day 1 to $91.6 \pm 4.7\%$ at day 7, as compared to the non-lyase scaffold, $24.9 \pm 4.9\%$ at day 1 to % 45.8 $\pm$ 4.2 % at day 7. In case of the cell perimeter, the difference with and without the lyase was about two times at day 7.
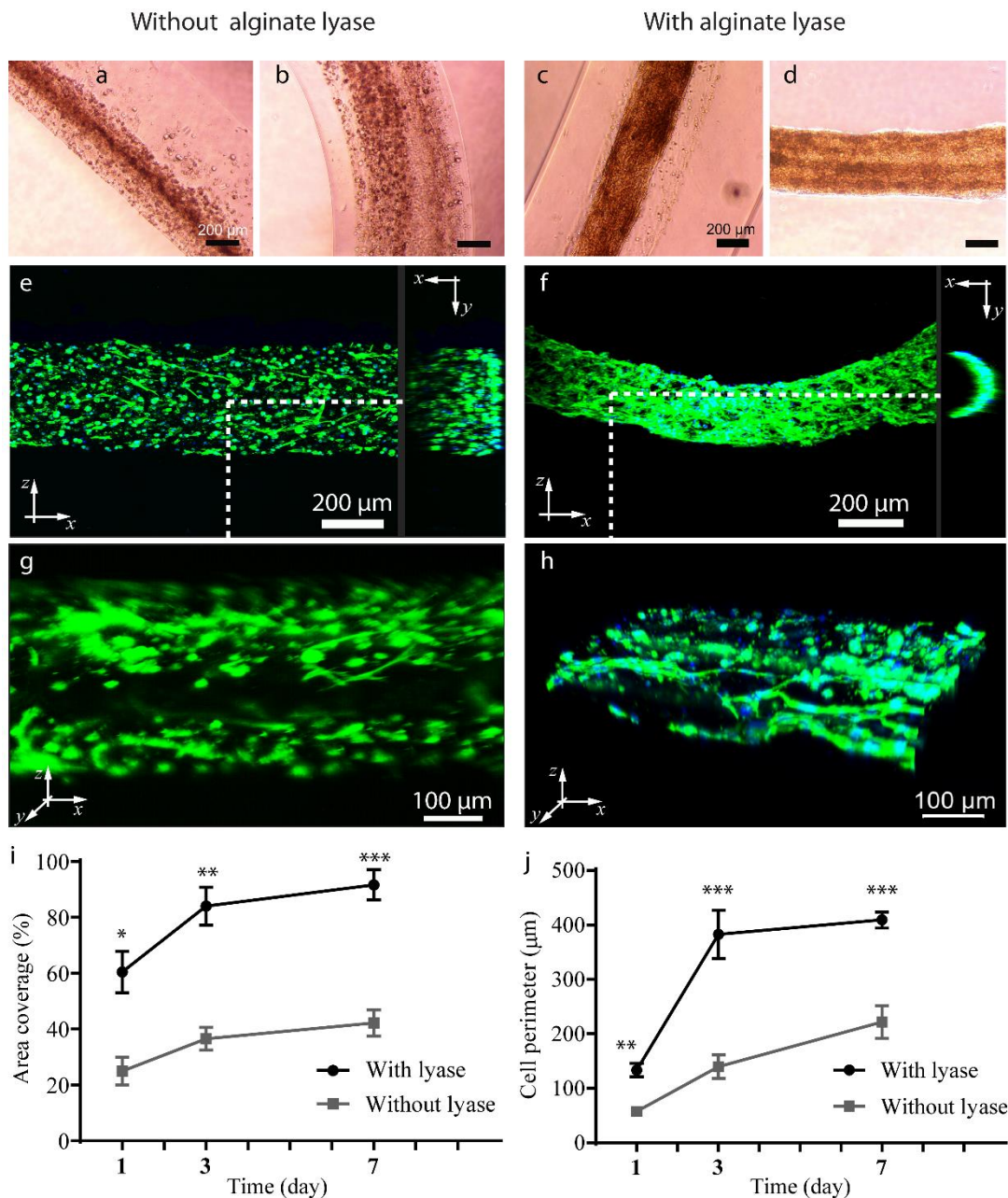
Figure 14. The HUVECs scaffold culturing without and with the alginate lyase. The bright-field images (a - b) without and (c - d) with the alginate lyase. (e) No hollow formation in one line region in case of no alginate lyase at day 3. (f) The hollow channel in one line region after 3 days culturing with the alginate lyase. The four lines region (g) without the alginate lyase and (h) with the alginate lyase (green: F-actin, blue: DAPI). (i) The area coverage according to the culturing time in both cases (* $p < 0.05$, ** $p < 0.01$, *** $p < 0.001$ comparing between with lyase and without lyase, n = 3). (j) The cell perimeter according to the culturing time in both cases, (** $p < 0.01$, *** $p < 0.001$ comparing between with lyase and without lyase, n = 100).
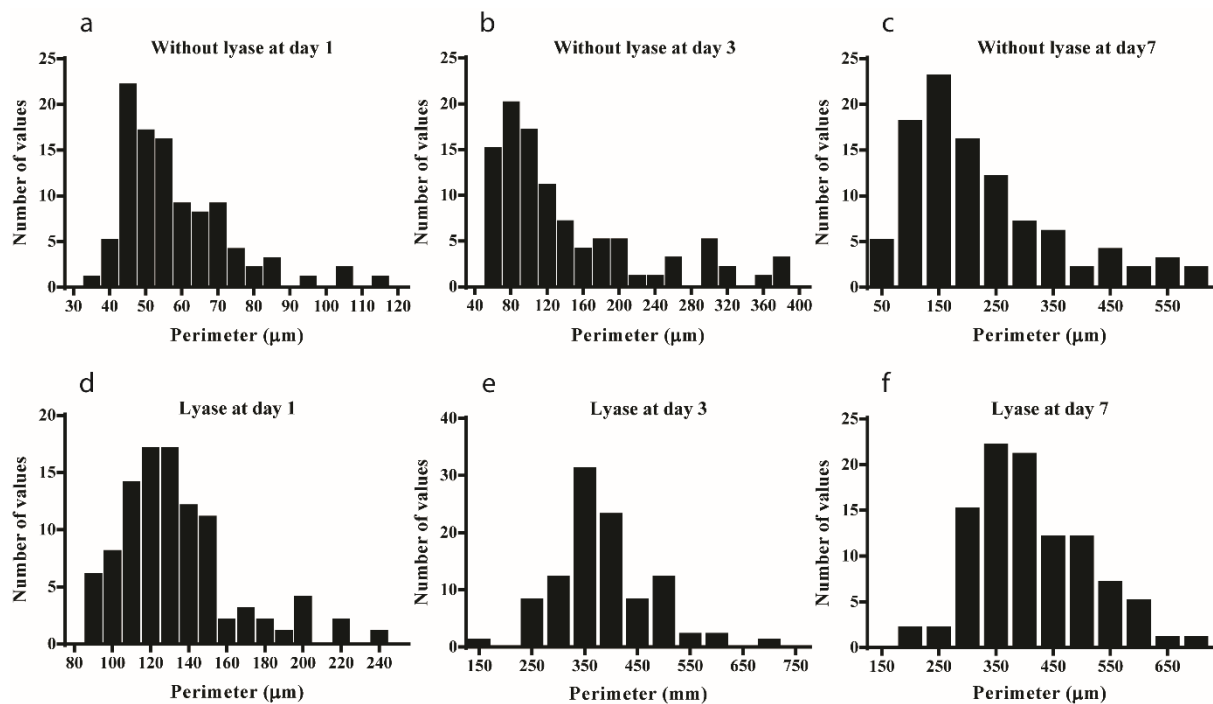
Figure 15. The HUVEC perimeter distribution. The HUVEC perimeter distribution without any alginate lysis for (a) 1 day, (b) 3 days, and (c) 7 days, respectively. The HUVEC perimeter distribution with the alginate lysis for (d) 1 day, (e) 3 days, and (f) 7 days, respectively. The number of samples is 100.

2.4.4 Microvascular network formation

Endothelial cells constitute the inner side of all vessel types as a monolayer, named as endothelium [70-73]. Adjacent endothelial cells link each other through inter-endothelial junctions, which are categorized as adherens junctions, tight junctions and gap junctions. These junctions play an essential role in tissue integrity, barrier function and cell–cell communication, respectively. The HUVEC scaffold cultured with alginate lyase expressed CD31 (a biomarker of platelet endothelial cell adhesion), ZO-1 (a biomarker of the tight junction), and VE-cadherin (a biomarker of the adherens junction) as shown in Fig. 16 a – c, respectively. The presence of these markers indicated the junctions among adjacent cells and the maturity of endothelial cells to form the vascular network [74, 75].
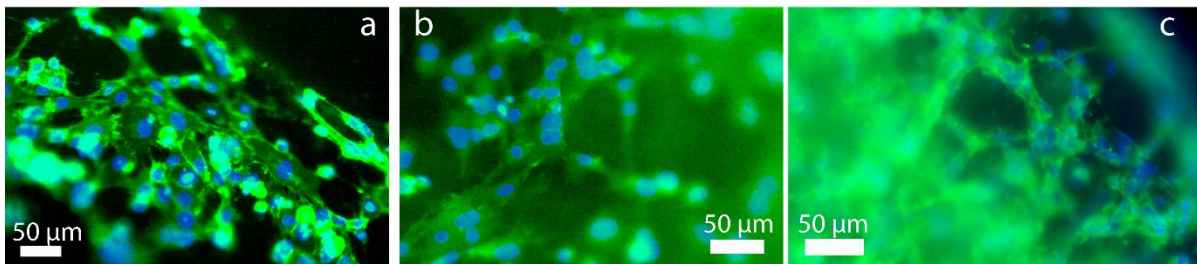
Figure 16. The immunofluorescent staining with (a) CD31 (green) - a biomarker of platelet endothelial cell adhesion, (b) ZO-1 (green) – a biomarker of the tight junction, and (c) VE-cadherin (green) - a biomarker of the adherens junction, in the HUVECs scaffold after 3 days culturing with the alginate lyase. The blue is DAPI.

The lyase-culturing HUVEC scaffold with high cell density (8×10^6 cells/mL) showed much more angiogenic sprouting in the one-line region and more cell-cell network formation in the four-line region than the non-lyase scaffold (Fig. 17). Angiogenic sprouting number in the lyase culturing increased from about 10.4 ± 1.7 at day 3 to 16.2 ± 1.9 at day 9. Its sprout length increased

from 80.8 ± 11.1 μm at day 3 to 191.0 ± 25.8 μm at day 9 as well. Furthermore, the distance between vessels were almost less than 100 μm (Fig. 18) The formation of the dense microvascular networks demonstrates a potential for volumetric artificial tissue to overcome the maximum diffusion distance from micro-vessels, 200 μm. In contrast, in the lyase-less HUVEC scaffold cells were disconnected and presented no angiogenic sprouting. In case of the cell density is lower (1×10^6 cells/mL), the cells create sparse networks and do not exhibit any angiogenic sprouting (Fig. 19).
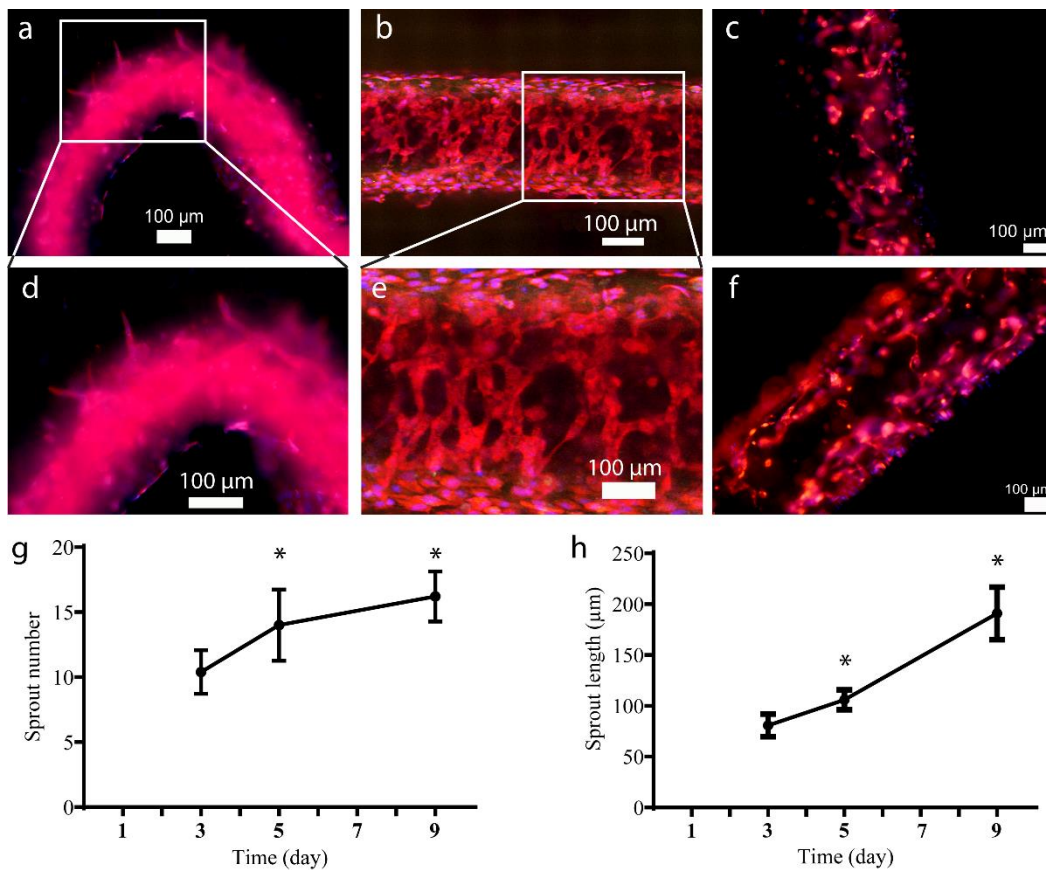
Figure 17. The fluorescent images of the RFP-HUVEC (a and d) in the one-line region and (b and e) in the four-line region after 3 days of culturing with the alginate lyase. (c and f) The fluorescent images of the RFP-HUVEC after 3 days culturing without any alginate lyase in the one-line and four-line region, respectively. The red is RFP-HUVEC. (g) The sprout number and (h) the sprout

27

length according to the culturing time with the alginate lyase, (* p < 0.05, compared with day 3, n = 5).
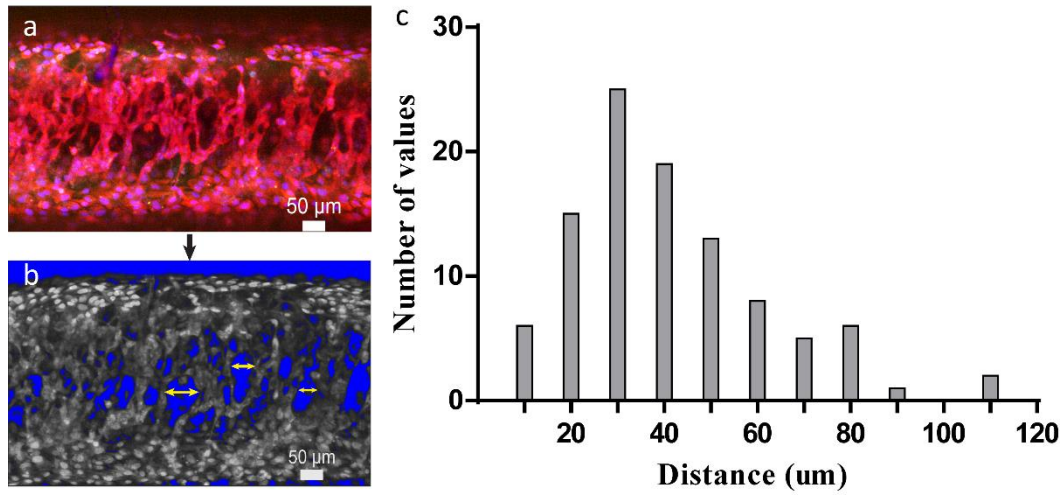
Figure 18. (a) The fluorescent image of the RFP-HUVEC microvasculature network. (b) The black-white image of image (a) was converted by ImageJ software. (c) The distribution of the distance between the vessels in the vasculature network on day 3. The results were conducted by ImageJ software (n = 100).
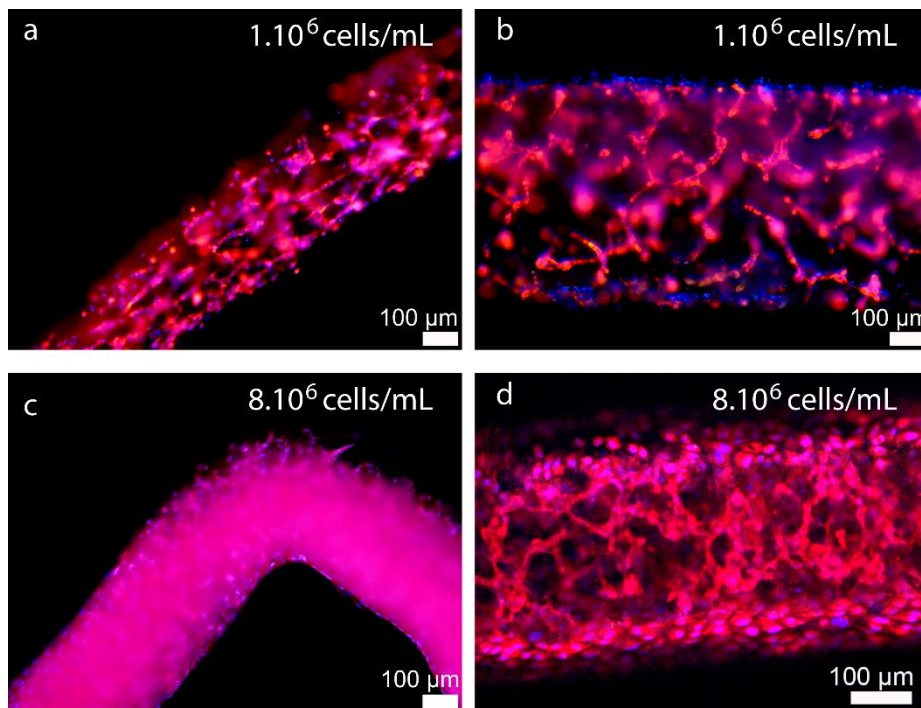
Figure 19. The growth of HUVECs scaffold in the one-line region (a) and in the four-line region (b) at the cell's density is 1×10^6 cells/mL, respectively. The growth of HUVECs scaffold in the one-line region (a) and in the four-line region (b) at the cell's density is 8×10^6 cells/mL, respectively.

2.4.5 Perfusability

Perfusion is one of the crucial properties in vasculature to induce a stable circulatory system or lymphatic system to an organ or tissue [76, 77]. To evaluate the perfusability of the fabricated microvascular networks different fluids, such as food dye, fluorescent microparticles, FITC-dextran, and whole mouse blood were pumped into the lyase-cultured HUVEC scaffold using a lab-made connector (Fig. 7a). As shown in Fig. 7b and c, food dye could successfully be perfused inside the HUVEC scaffold. After perfusing with red 5 um microparticles some of the microparticles, Fig. 20b, could be found adhering to the inside of the one-line region. Likewise, FITC-dextran 70 kDa was perfused through the fabricated vasculature network and out of the HUVEC scaffold without leakage. In the four-line region, some FITC-Dextran (the green one in Fig. 21 b – d) were found after pumping. After pumping whole mouse blood, some red blood cells (the pink arrows in Fig. 22c), analogous to the microparticle perfusion, were found on the inside of the lumen in the network region. The perfusion experiments demonstrate that the achieved vasculature network demonstrated an intact endothelium with considering the expressed biomarkers and its ability to confine the perfused fluids inside the lumen.
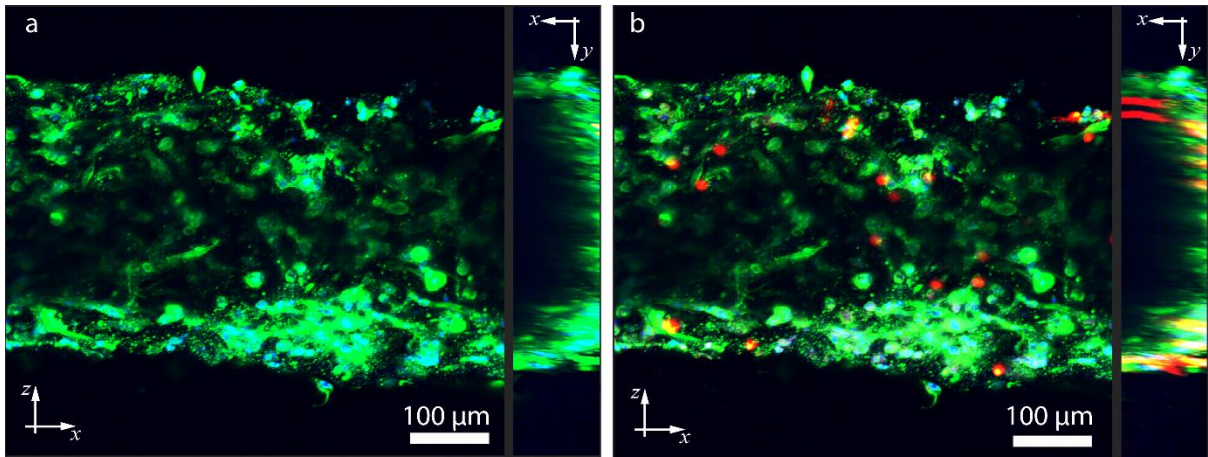
Figure 20. The confocal microscope images of the one-line region (a) before and (b) after pumping the fluorescent microparticles. The red, green, and blue are fluorescent microparticles, F-actin, and DAPI, respectively.
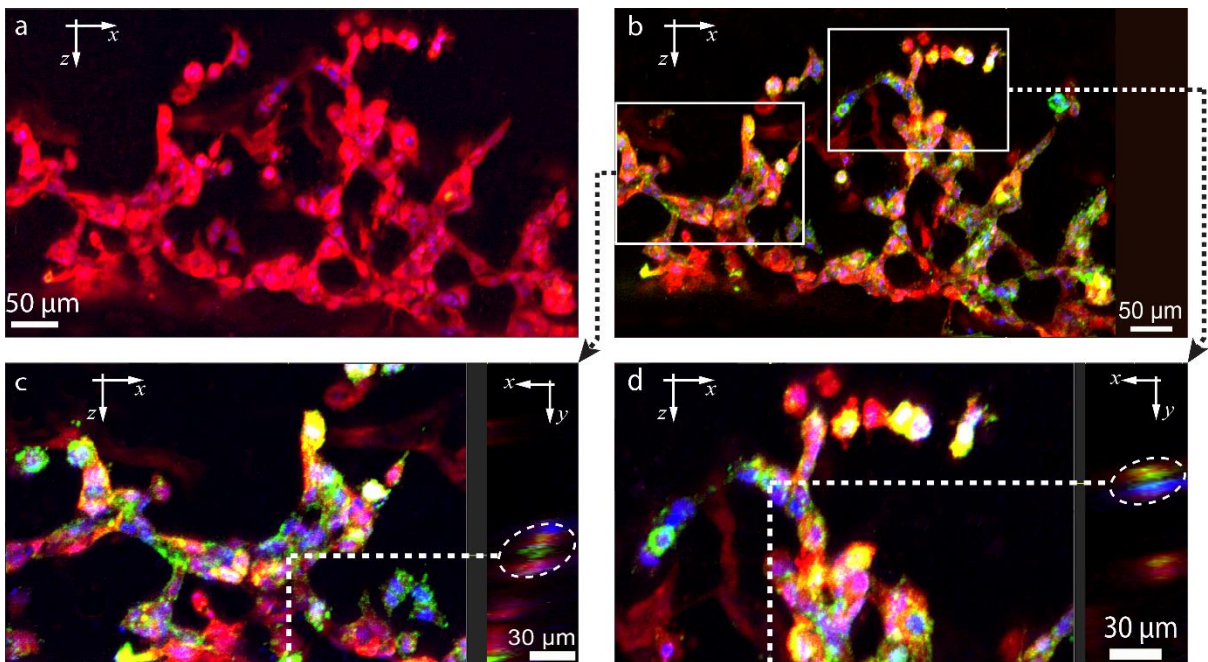
Figure 21. The confocal images in the microvascular network (a) before and (b) after pumping the FITC-Dextran 70 kDa. (c and d) The remaining FITC-Dextran inside the capillary. The green, red, and blue are FITC-Dextran, RFP-HUVEC, and DAPI, respectively.
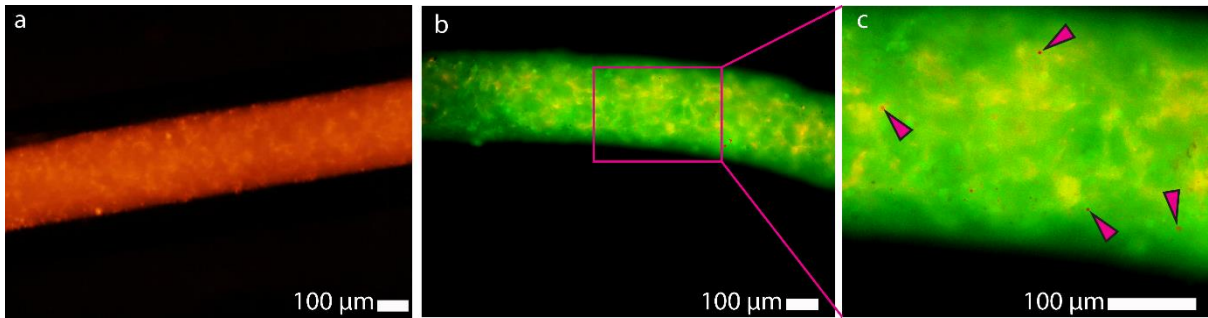
Figure 22. The perfusability test of the HUVECs microvascular network with mouse blood. (a) The fluorescent images of the RFP-HUVEC microvascular network scaffold (light red) before pumping. (b - c) The fluorescent images in the network region after pumping mouse blood. The pink arrows point the red blood cells of the mouse blood. The dark red is a red blood cell. The green is cell tracker dye.

2.4.6. 14 days Subcutaneous Implantation

To estimate implantablity of the HUVEC network scaffold, it was grafted under mouse dorsal skin as shown in Fig. 23 a – e. After surgery, the transplanted region recovered quickly with neither swelling nor inflammation. The operated skin was mostly recovered after 7 days, and hair regrew after 14 days. Under bright field microscopy, blood vessels in the extracted tissue were observed as well (Fig. 23 f – h).

31
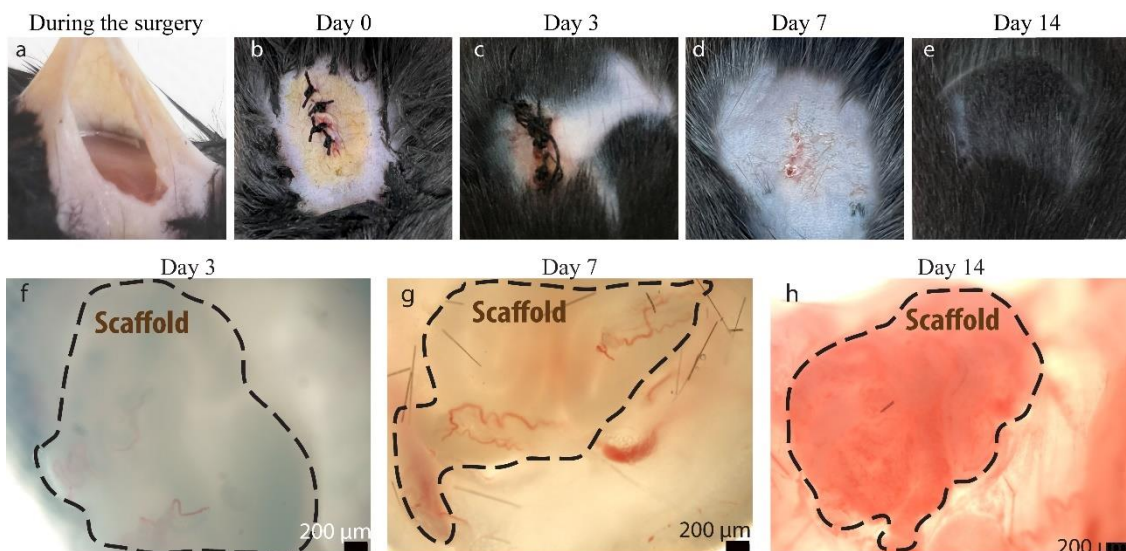
Figure 23. The implantation of the cultured HUVEC scaffold into the mouse. (a) The scaffold was placed under the skin on the back of the mouse during the surgery. (b) The skin was sutured after the implantation. The implanted areas for (c) 3 days, (d) 7 days, and (e) 14 days after the surgery. The bright-field images of the tissues extracted from the mouse at (f) day 3, (g) day 7 and (h) day 14 from the surgery, respectively. The grown hair was removed before extracting the tissue to observe under a microscope at day 14.

Histological analysis with hematoxylin and eosin (H&E) staining (Fig. 24) and Masson's trichrome staining (Fig. 25) further showed efficient incorporation of the implanted scaffold into the host tissue. As time went from the implanting surgery, red blood cells were observed in smaller lumens (Fig. 24 d – f). At day 3, the smallest lumen having red blood cell is 12.1 µm in diameter. The smallest lumen decreased as 8.1 µm at day 14. These findings supposed that the plural microvessels inside the implanted scaffold evolved from empty tubular structures to functional blood-carrying microvessels and the implanted scaffold formulated with human endothelial cells anastomosed with the existing vasculature of the host. Furthermore, Masson's trichrome staining showed that the collagen fibers - as the representative of the extracellular matrix surrounding the cells site - considerably increased within the grafted tissue after 14 days implantation (Fig. 25). These results were an indicator of a good incorporation to the host tissue.
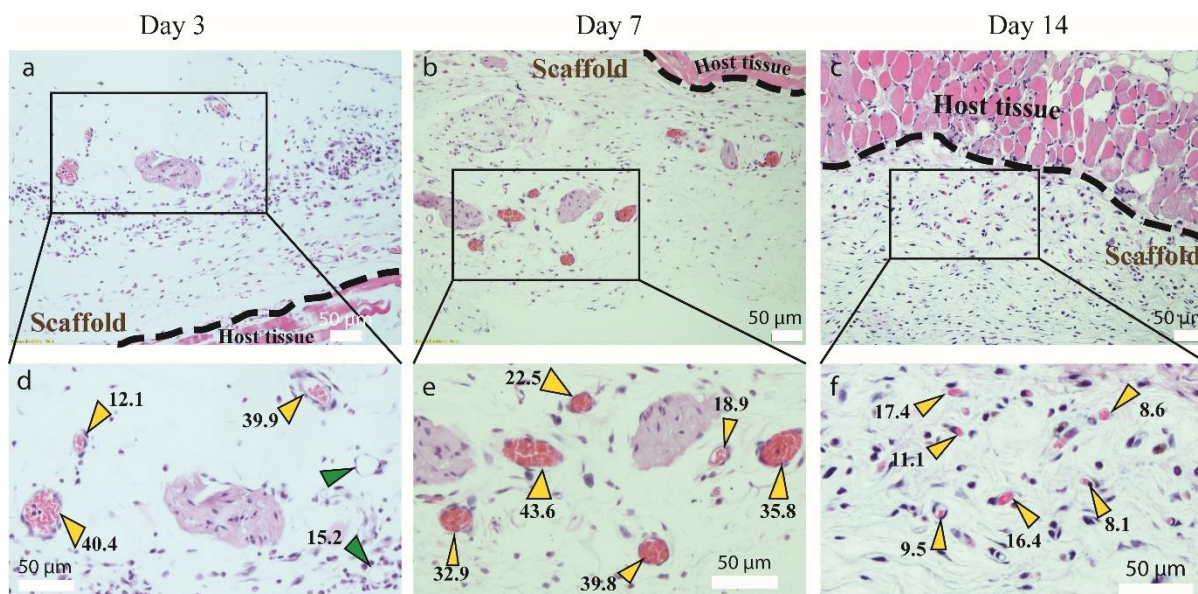
Figure 24. The hematoxylin and eosin (HE) staining images of the scaffold implanted in the mouse dorsal for (a, d) 3 days, (b, e) 7 days, and (c, f) 14 days, respectively. The yellow arrow points micro-vessel carrying red blood cells. The numbers are diameters of the lumens. The green arrow indicates the empty lumens. The pink is an extracellular matrix. The purple is nuclei. The bright red is red blood cell.
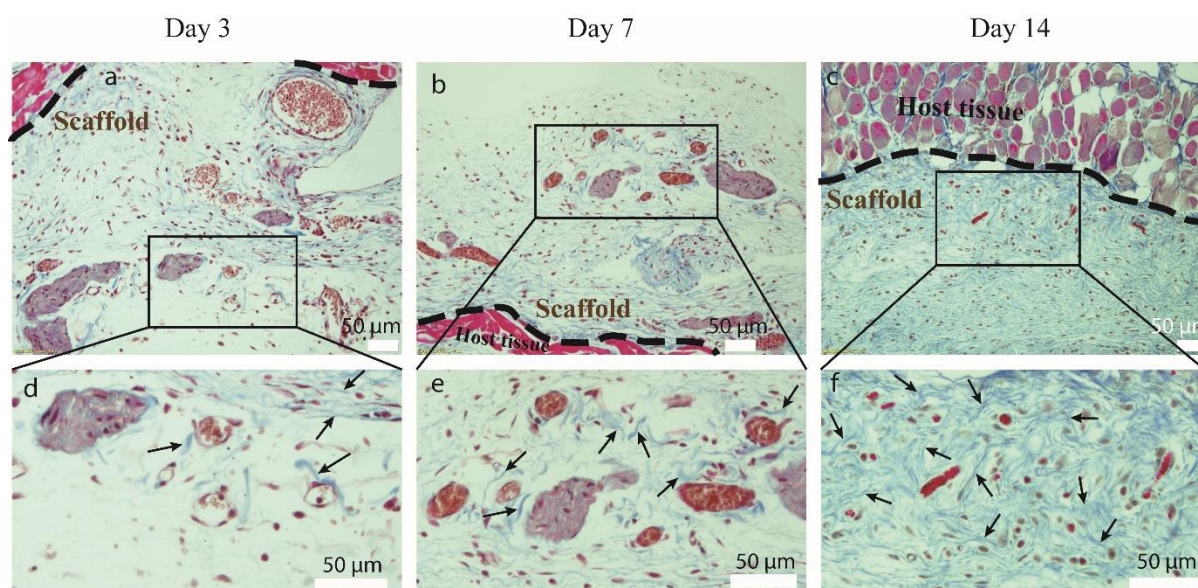
Figure 25. The Masson's trichrome staining images of the scaffold implanted in the mouse dorsal for (a, d) 3 days, (b, e) 7 days, and (c, f) 14 days, respectively.

The micro-vessels can be recognized as lumen structures carrying red blood cells. The pink is cytoplasm. The black is nuclei. The blue is collagen fibers and extracellular matrix. The black arrowhead points to collagen fibers. The red is red blood cell.

Chapter 3: Ultrasound patterning for fabrication of vasculature artificial liver scaffold

3.1. Background

The liver is the largest internal organ, which plays a vital role in different physiological and metabolic functions. In recent years, the demand for liver transplantation far exceeds the limited supply of donor organs, leading to long waiting times and high mortality rates for patients with end-stage liver disease [78, 79]. The development of 3D-engineered liver tissue could potentially provide an unlimited source of functional hepatic tissue, alleviating the shortage of donor organs.

The assembly of 3D structures allows for mimicking the native structure of the liver within a biocompatible material. Different manufacturing techniques have been used to 3D print hepatic-like structures, including biomimicry and mini-tissue building blocks. For example, cells of the hepatic cell line (HepG2) were printed as multilayered with sodium alginate. However, using a high extrusion pressure from the printing device decreased cell viability [80]. Another widely utilized approach in developing 3D platforms for *in vitro* culture involves seeding cells into 3D scaffolds. 3D scaffolds can be developed by using biological ECM derived from the decellularization of tissues and organs. Decellularized liver hydrogel can improve hepatocyte survival and higher metabolic activity because it is capable of providing a more appropriate microenvironment should be developed for the use of hepatocytes in liver tissue engineering, and liver transplantation [81, 82].

Recent research has shown that co-culturing fibroblasts, human umbilical vein endothelial cells (HUVECs), and hepatocytes can improve the functioning of hepatocytes and the use of two-dimensional (2D) patterning to induce interaction among cells [83, 84], but these studies were limited to the 2D environment. To address this limitation, other approaches have been explored. One such approach involves the encapsulation of hepatocytes using a heparin-

based hydrogel and 3D cell culture with hepatic cell sheets [85, 86]. However, these techniques cannot be used to efficiently mimic 3D constructs of native livers. Also, Mao et. al applied digital light processing (DLP) bioprinting with GelMA/dECM cell-laden bio inks for the fabrication of liver microtissue [87]. Nevertheless, the UV light during the printing process will affect cell viability.

In this chapter, applying the properties of USW, the scaffold with a basic unit structure of liver tissue was generated. This structure includes branched blood vessels surrounded by hepatocyte clusters. Culturing the fabricated scaffold with alginate lyase enabled the ECs to form a microvasculature network and the functionality of hepatocyte cells was demonstrated. The co-culture of hepatocytes and endothelial cells enhanced the function of liver cells. It demonstrated the potential for implantation, improving biological processes, and even manufacturing full-size artificial liver tissue.

3.2. Theory and concept

The USW at frequency 2 MHz in two types of square glass capillaries (400 µm and 800 µm) could generate a transition from one focused cell stream to four cell streams of HUVECs and vice versa. Same as Chapter 2 (section 2.2), When applying 2 MHz ultrasound in a 400 µm square-shaped glass capillary, a half-wavelength standing wave was generated. When the capillary was doubled to 800 µm, the square capillary supported a full wavelength resonance in both the x- and y-directions and hence four pressure nodes were generated in the capillary cross-section, located $\lambda/4$ from the channel side walls.

When HUVECs were mixed with HepG2 aggregates, based on the difference of the acoustic contrast factor (ϕ), these two cell types will move in two different directions. The HUVECs with a positive contrast factor will move toward the nodes. Meanwhile, HepG2 aggregates with a negative contrast factor

will move toward the position of the antinode (on both sides of the tube wall) [88] (Figure 26).
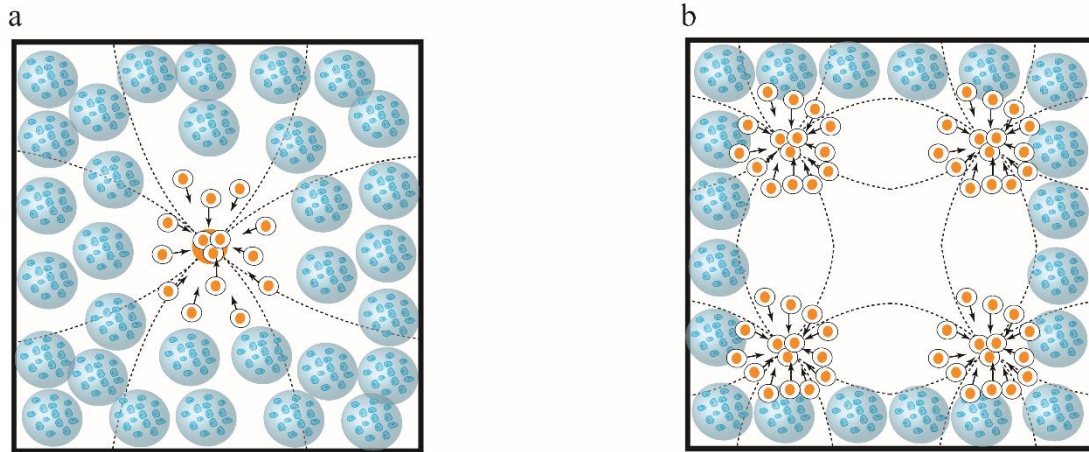
Figure 26. Schematic of the standing wave pattern in the capillary cross-section when actuated (a) at 2 MHz in 400 µm square-shaped glass capillary, (b) at 2 MHz in the 800 µm square-shaped glass capillary with the single cells move forward to the nodes position, and the cell aggregates move forward to the antinode position.

This will result in HUVEC cells being patterned into a branched structure, and HepG2 aggregates will surround this branched structure (Fig. 27). After fabrication, the scaffolds will be cultured with alginate lyase enzyme for micro-vascular network formation and to improve liver cell function.
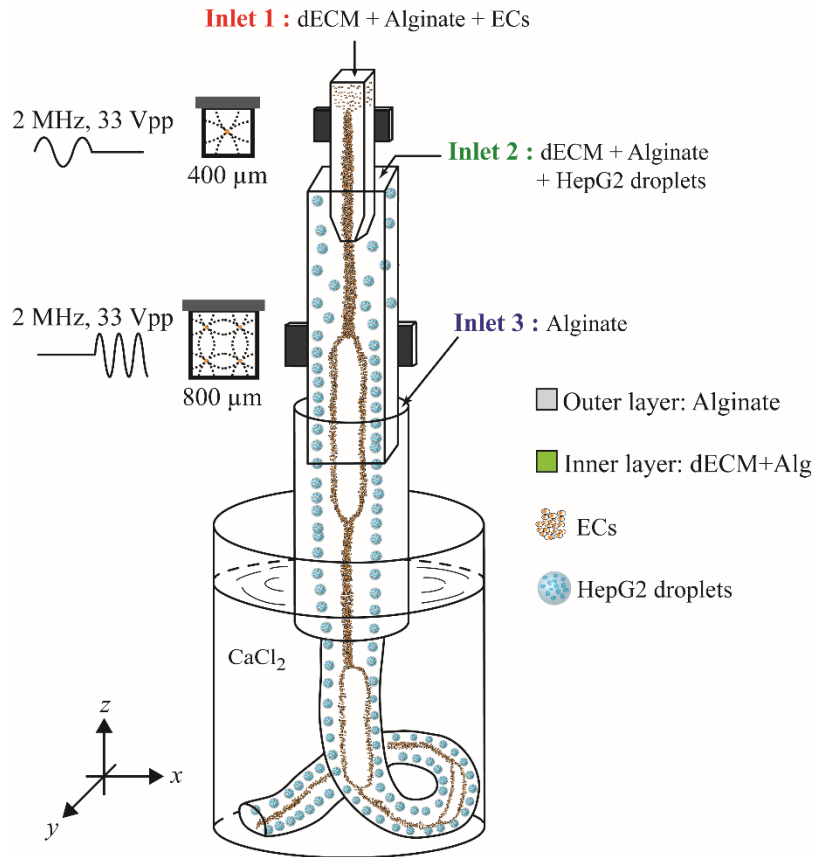
Figure 27. Schematic of the artificial liver scaffold fabrication with HUVECs patterning in hydrogel using ultrasound.

3.3. Materials and methods

3.3.1 Hydrogel preparation

350 milligram liver dECM (L-dECM) powder and 200 mg pepsin (Sigma-Aldrich, St. Louis, MO, U.S.A.) dissolved in 5 mL acetic acid (Sigma-Aldrich, St. Louis, MO, U.S.A.) and DI water to make 35 mg/mL concentration L-dECM of 100 mL total volume solution. The solution was stirred for 72 – 96 hours at room temperature (RT). After that, the dissolved L-dECM was centrifuged at 3000 rpm for 15 min. The supernatant was carefully transferred into other conical tubes, and then the remaining non-dissolved components were discarded. The tubes containing dissolved L-dECM were kept in storage at 2 – 8 °C.

For L-dECM neutralization and dilution, the 35 mg/mL L-dECM was mixed with 10 M and 1M NaOH (Sigma-Aldrich, St. Louis, MO, U.S.A.) and 10X PBS (10% of the total volume) to adjust pH range from 7.2 to 7.5 and 25 mg/mL L-dECM concentration. The final hydrogel for acoustic pattering was a mixture of sodium alginate (MERCK, Madison, NJ, U.S.A.) (0.5% w/v) and L-dECM (25 mg/mL) at a ratio of 1:9. All these steps were processed on ice to avoid gelation.

3.3.2 Cell culture

HepG2 and human umbilical vein cell line (EA.hy926) were purchased from ATCC (ATCC, U.S.A.). Cell culture medium included Dulbecco's Modified Eagle Medium (DMEM, Gibco, U.S.A.), 10% Fetal Bovine Serum (FBS, Gibco, U.S.A.) and 1% penicillin/streptomycin (Sigma-Aldrich, St. Louis, MO, U.S.A.). Both cells were seeded on cell culture polystyrene dishes and incubated at 37 °C and 5% CO_2. An IX53 inverted microscope (Olympus, Japan) was used to observe the cell growing.

3.3.3 HepG2 aggregates fabrication

HepG2 cells were mixed with a mixture of L-dECM and sodium alginate (ratio – 9:1). This specific ratio was chosen to optimize the supportive environment provided by the L-dECM while maintaining the structural integrity conferred by the sodium alginate. Then the cell-hydrogel mixture was extruded through a nozzle with a size of 75 ± 3 μm and the flow rate was 20 μL/min. The HepG2-hydrogel droplets were pumped into a baker of 0.1M $CaCl_2$ (MERCK, Madison, NJ, U.S.A.) for cross-linking. Following the cross-linking, the fabricated HepG2-hydrogel droplets were cultured in a suitable culture medium over a period of four days. This culture period was critical for the formation of HepG2 aggregates within the hydrogel droplets (Fig. 28).
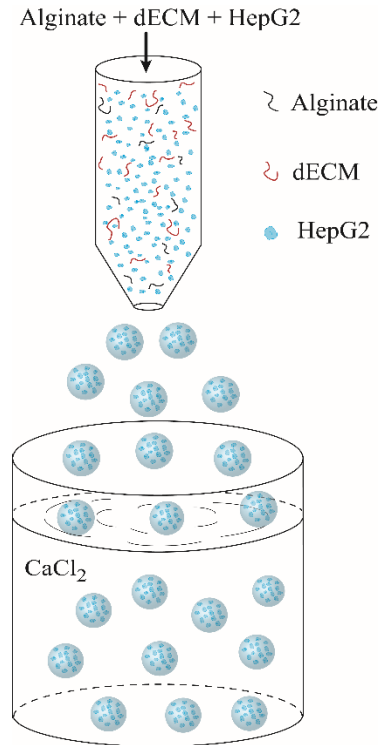
Figure 28. Schematic of the HepG2 aggregates formation by encapsulating HepG2 cells inside hydrogel droplets.

3.3.4 Artificial liver scaffold fabrication using ultrasound standing wave

As shown in Figure 27, 1 mm thick ultrasound transducers (MEGITT A/S, Kvistgaard, Denmark) glued to a 400 µm and 800 µm square-shaped glass capillaries (VitroCom, NJ, U.S.A.), respectively. The device has three inlets. The mixture of sodium alginate and L-dECM was mixed with HUVECs and was pumped into inlet 1. The same ratio of L-dECM and alginate was mixed with HepG2 aggregates and was supplied into inlet 2. Sodium alginate (1% w/v) was only injected into the inlet 3. The flow rate for inlet 1 was 30 µL/min, inlet 2 was 30 µL/min and inlet 3 was 300 µL/min. The outlet was immersed into a beaker of 300 mM $CaCl_2$ for cross-linking. The scaffold was then incubated for at least 10 minutes at 37°C to allow dECM gelation.

3.3.5 Microvascular network in artificial liver scaffold formation

The extruded artificial liver scaffolds were cultured in the conventional culture medium described previously for one day at 37 °C and 5% CO_2 to maintain the extruded three-layered structures intact. After one day of the conventional culturing, alginate lyase enzyme (MERCK, Madison, NJ, U.S.A.) was added into the culture media at a final concentration of 0.1 unit/mL. The role of this enzyme is to selectively degrade the calcium alginate components of the scaffolds, which is essential for creating pathways that allow the HUVECs to migrate and integrate into the scaffold structure. To ensure the continuous and effective degradation of alginate, the alginate-degrading media was replaced every two days. This regular replacement is crucial to maintain the enzymatic activity and to prevent the accumulation of degradation byproducts, which could potentially inhibit cell migration or affect scaffold integrity.

3.3.6 Cell staining

After scaffold fabrication, at 6 hours and 24 hours, the cell scaffolds were stained with LIVE/DEAD staining solution. The staining solution was composed of 0.2% ethidium homodimer-1 (EthD-1 2 mM) in dimethyl sulfoxide (DMSO)/H_2O 1:4 (v/v); 0.05% calcein-acetoxymethyl (calcein-AM 4 mM) in anhydrous DMSO (LIVE/DEAD Viability/Cytotoxicity Kit, for mammalian cells, Molecular Probes, Eugene, OR, USA), and was diluted in 1X phosphate-buffered saline (PBS) (D8662-500ML, MERCK, Madison, NJ, USA). Before and after staining, the cell scaffolds were lightly washed with 1X PBS buffer (3 times, 1–3 min per time) to remove media and staining solution prior to being examined with a 4X objective lens on an Olympus BX53 digital upright microscope (Olympus, Japan). Five images were analyzed using ImageJ software (Fiji, NIH Image, U.S.A.). For the purpose of calculating cell viability, the fluorescent signal of the labeled cells was separated into two channels: a red channel representing dead cell signal and a green channel representing living

cell signal. ImageJ was used to assess the strength of each channel. The percentage viability was calculated from the measured signal intensity using the green intensity to total intensity ratio:

$$Cell\ viability = \frac{green\ gv}{green\ gv\ +\ red\ gv} \times 100\%$$

3.3.7 Proliferation assay

During culturing, after 24 hours of conventional culturing, on day 3 and day 7 after adding alginate lyase enzyme, the liver scaffolds were plated in a 96-well plate with 100 μL of medium per well. Then, 20 μL of CellTiter 96 AQueous One Solution Cell Proliferation Assay solution (Promega, Madison, WI, USA) containing a tetrazolium compound (3-[4,5-dimethylthiazol-2-yl]-5-[3-carboxymethoxyphenyl]-2-[4-sulfophenyl]-2H-tetrazolium; MTS) and an electron coupling reagent (phenazine ethosulfate; PES) was added, after which the scaffolds were incubated at 37 °C for 4 hours. The absorbance was quantified at 490 nm using a SpectraMax iD3 reader (Molecular Devices, San Jose, CA, USA). The experiment was repeated 6 times under the same conditions.

3.3.8 Albumin secretion and urea production

To assess albumin secretion, media samples were collected at different time points. The quantity of secreted albumin and produced urea were measured using a human albumin ELISA kit (Abcam, Cambridge, UK) and urea assay kit (ab83362, Abcam, Cambridge, UK), respectively. The results were determined at 450 nm and 570 nm, respectively, using a SpectraMax iD3 reader (Molecular Devices, San Jose, CA, USA).

3.3.9 Immunofluorescent staining

The artificial liver scaffold was fixed in 4% paraformaldehyde (Sigma-Aldrich, St. Louis, MO, U.S.A.) for 25 minutes at RT, permeabilized with 0.5% Triton-X100 (Sigma-Aldrich, St. Louis, MO, U.S.A.) for 5 minutes, and then treated with 5% bovine serum albumin (BSA) (Sigma-Aldrich, St. Louis, MO, U.S.A.) as blocking solution for 20 min at RT. The primary antibody CD31 (1:500) (ab9498, Abcam, Cambridge, UK), albumin (ab207327, Abcam, Cambridge, UK) were incubated with the treated scaffolds at 4 ℃ overnight. Subsequently, the scaffolds were incubated with a goat anti-mouse IgG (H + L) highly cross adsorbed secondary antibody, Alexa Fluor plus 488 (1:1000) (Thermo Scientific, Waltham, Massachusetts, U.S.A.) and Alexa Fluor® 594 (1:1000) (ab150080, Abcam, Cambridge, UK) for 120 minutes at RT. The nuclei were stained with 4′,6-diamidino2-phenylindole (DAPI) (NucBlue® Live ReadyProbes™ Reagent, Thermo Scientific, Waltham, Massachusetts, U.S.A.) for 15 minutes before imaging. The scaffolds were washed with 1X PBS buffer (3 time/5 min) between steps.

3.3.10 Imaging and Statistical analyses

The imaging and analysis methods were similar to chapter 2, section 2.2.10.

3.4. Results and discussion

3.4.1 HepG2 aggregates culturing

The cultivation of hepatocytes as aggregates could potentially improve hepatocytes' performance, allowing enhanced cell-cell contacts in a three-dimensional context. Compared to traditional two-dimensional cell cultures, cell aggregates are more typical of liver tissue and can be thought of as micro-tissues. Furthermore, hepatocytes assembled into three-dimensional cell

aggregates may be used as functional building blocks to assemble bigger structures [89, 90].

The aggregation procedure was observed at different cell numbers as 1×10^6 (group 1), 3×10^6 (group 2), and 5×10^6 (group 3) cells/mL of HepG2. Despite this hepatocellular carcinoma cell line is less suggestive of the in vivo experiment, but this cell is user-friendly, robust, and aggregates easily while maintaining some hepatocyte-specific functions. As shown in Fig. 28, for both cases, aggregate formation started from day 1. In addition, the aggregate diameters were measured. After 4 days after culturing, aggregate diameters increased from 23.3 ± 6.2 μm to 41.1 ± 11.7 μm for 1×10^6 cells/mL, from 23.4 ± 7.1 μm to 50.3 ± 16.5 μm for 3×10^6 cells/mL, and from 28.9 ± 6.6 μm to 77.5 ± 19.1 μm for 5×10^6 cells/mL.

Figure 29 also showed that the diameter distribution in the three groups was significantly different. On day 1, while group 1 and group 2 had a diameter of aggregates were distributed mainly in the range of 15 - 25 μm, in group 3, the aggregates were distributed in the range of 20 - 35 μm. By the fourth day, this distribution was clearer, and group 3 had the best results with the size distribution in the range of 70 - 90 μm. The results proved that, as the cell concentration increased, the number and diameter of aggregates also increased. Furthermore, live/dead staining of the different aggregates indicated excellent cell viability in the aggregates with cell viability of HepG2 aggregates found to be over 90% (Fig. 30) at day 4 of culturing with the structure of a solid spherical aggregate of HepG2 cells (Fig. 31).
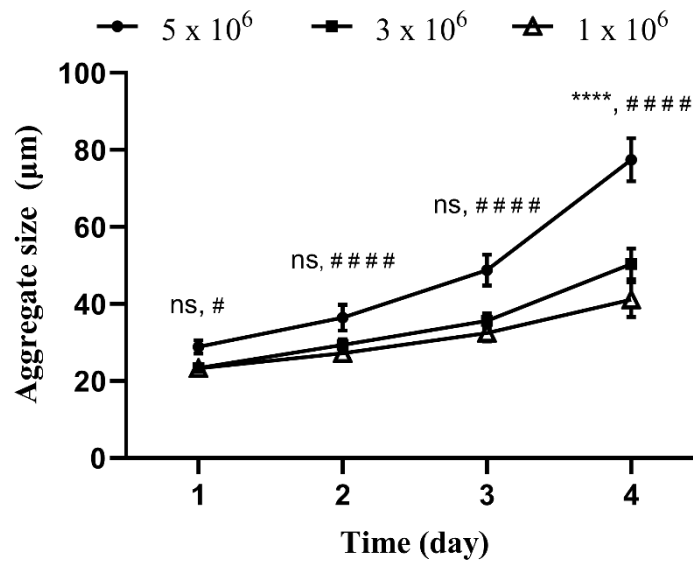
Figure 29. The relationship between the HepG2 cells number and the aggregate diameter after 4 days of culturing, n = 100 (# p < 0.05, ****, #### p < 0.0001).
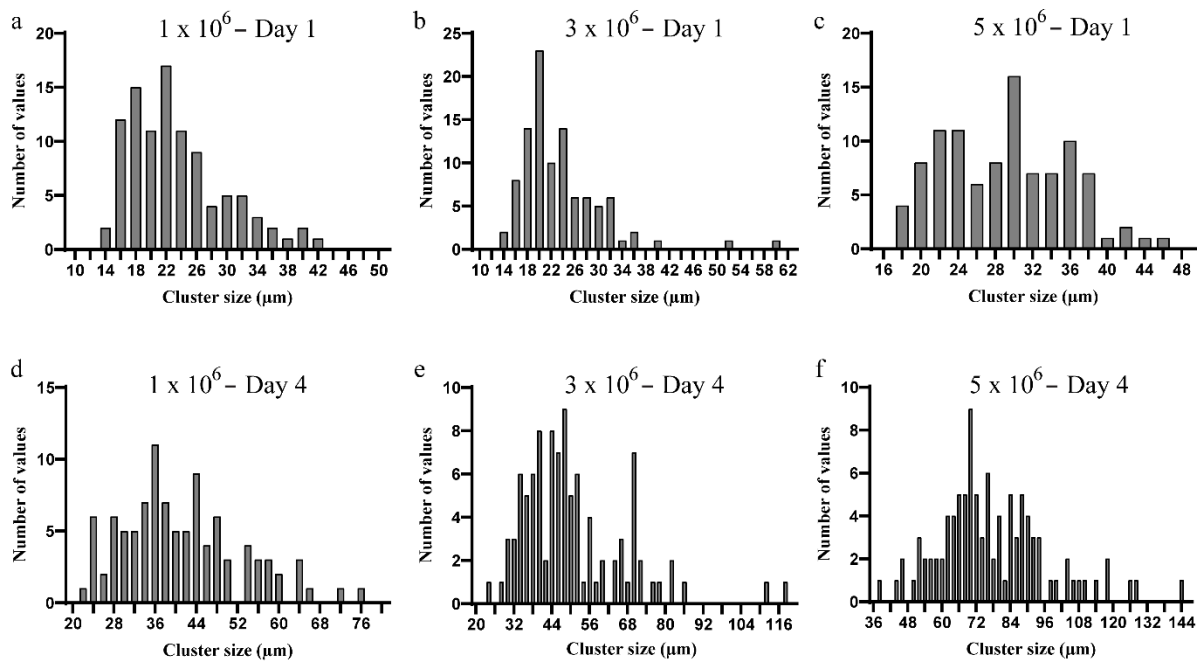
Figure 30. The HepG2 aggregate diameter distribution. The HepG2 aggregate diameter distribution at day 1 of culturing for (a) 1×10^6 cells/mL, (b) 3×10^6 cells/mL, (c) 5×10^6 cells/mL, respectively. The HepG2 aggregate diameter

distribution at day 4 of culturing for (a) 1×10^6 cells/mL, (b) 3×10^6 cells/mL, (c) 5×10^6 cells/mL, respectively. The number of samples is 100.
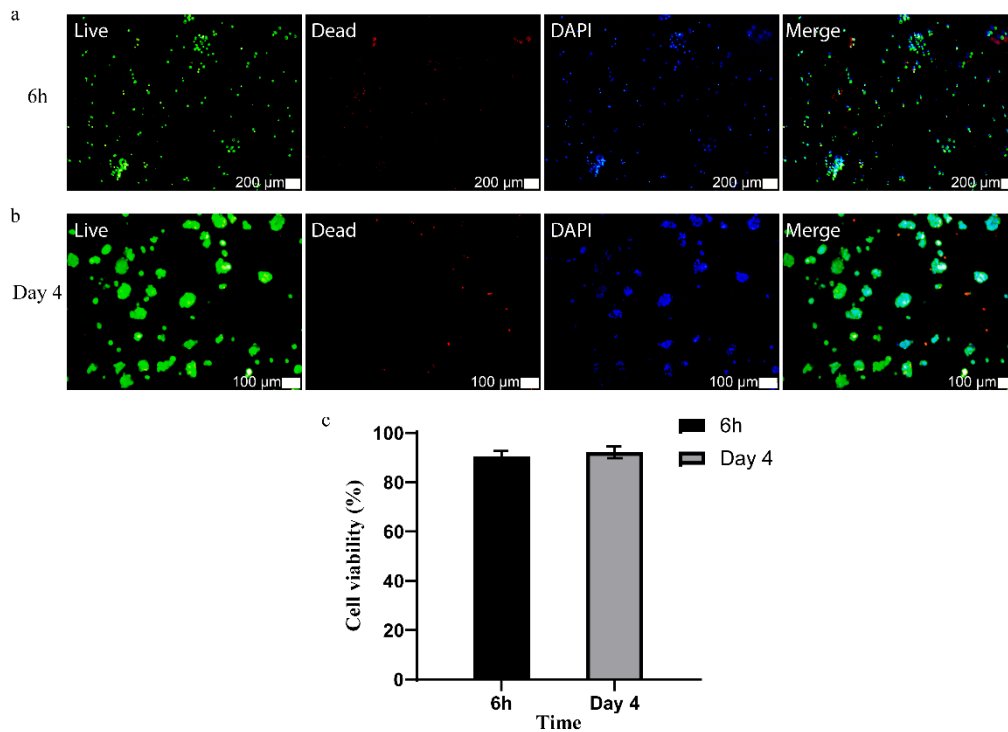
Figure 31. The live and dead fluorescent images of the HepG2 aggregates after 6 hours and after 4 days of culturing. The green is a live cell. The red is a dead cell. The blue is DAPI.
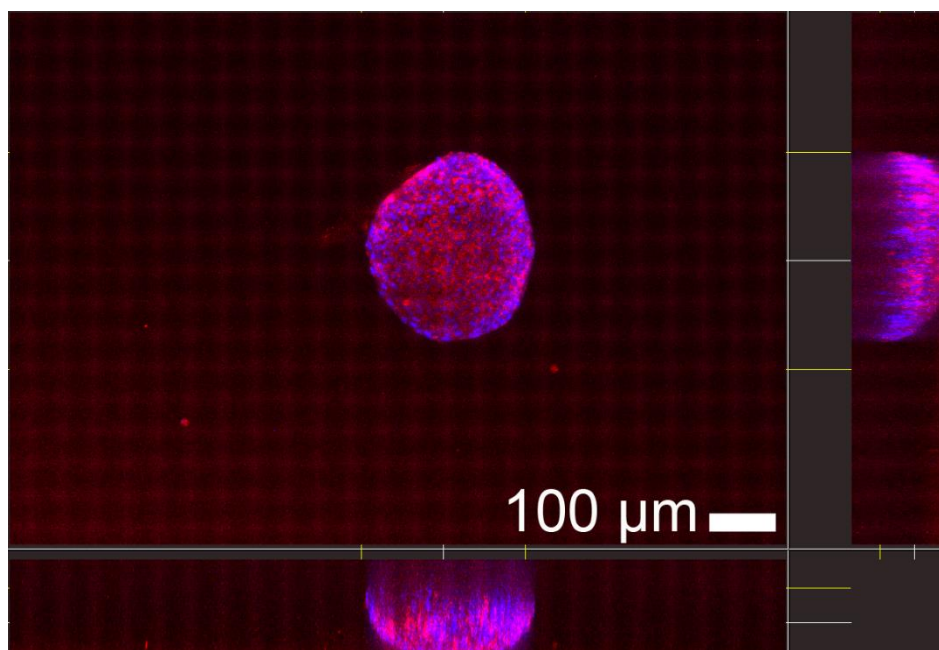
Figure 32. The confocal immunofluorescent staining image of HepG2 aggregate.

3.4.2 Artificial liver scaffolds formation with branched structures of HUVECs

For three-dimensional vascularized liver scaffold formation, the cultured HepG2 aggregates were mixed with HUVECs for ultrasonic patterning. HUVECs with positive contrast factor were patterned alternating in a single line and in four lines (Fig. 32) to form branched structures within the hydrogel, whereas HepG2 aggregates with negative contrast factor moved towards the position of the antinode, where are both sides of the tube wall. The results indicated that this technique has the potential to fabricate the basic unit structure of liver tissue, which includes branched blood vessels surrounded by hepatocyte clusters.
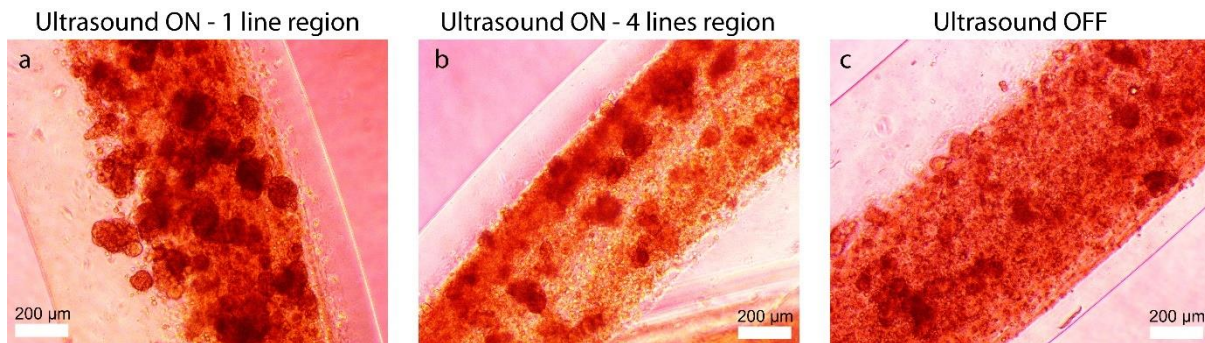
Figure 33. Artificial liver scaffolds formation with branched structures of HUVECs. (a) The bright-field microscope images of one line region. (b) The bright-field microscope images of four lines region. (c) The bright-field microscope images of ultrasound off region.

3.4.3 Microvascular network formation in the artificial liver scaffolds

Based on the results shown in Figure 33, the cell viability of both groups was increased and reached a value of about 90% after 1 day of fabrication (Fig. 33 a-d). In addition, the proliferation of fabricated scaffolds in 7 days was

48

shown in Fig. 33e. It can be seen that the scaffold with HepG2 aggregates and HUVECs proliferated more rapidly than others, almost 2-folds time when compared to only HepG2 cells group.

HUVECS spreading in the artificial liver scaffolds was visualized using immunofluorescent staining of CD31 (green), which is a biomarker of platelet endothelial cell adhesion, and the maker of HepG2 is albumin (red) (Fig. 34). On day 1, some of the HUVECs retained their original round shape inside the hydrogel. After 3 days of culturing with alginate lyase enzyme, the scaffold with HepG2 aggregates, HUVECs exhibited robust growth compared to the group of single HepG2 cells.

CD31 and albumin staining were also performed under a confocal fluorescence microscope, which showed the lumen formation of HUVECs in one line region (Fig. 35a), and the mature to form the vascular networks in the four-line region (Fig. 35c). The HUVECs migrated and spread into HepG2 aggregates (Fig. 35b, d). These outcomes demonstrate that in the printed scaffolds, HUVECs have the potential to support and enhance the growth of liver cells in artificial liver tissue.
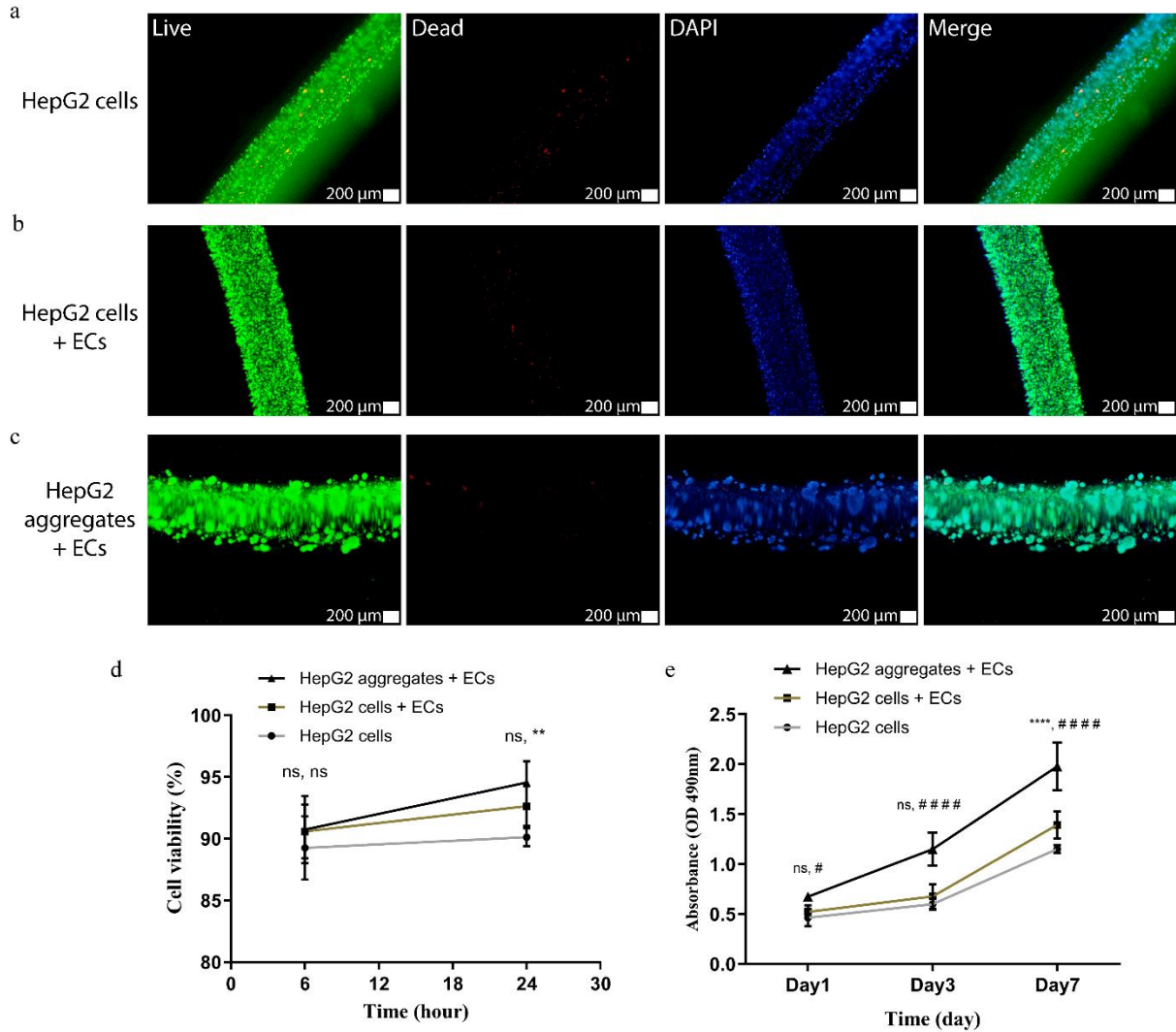
Figure 34. Evaluation of cell viability and cell proliferation of the fabricated scaffolds. The live and dead fluorescent images of scaffolds with (a) only HepG2 cells, (b) HepG2 cells + HUVECs, and (c) HepG2 aggregates + HUVECs after 24 hours of fabrication. (d) The cell viability (** $p < 0.01$). (e). Cell proliferation determined via CellTiter 96 AQueous one solution cell proliferation assay analysis after 7 days of culture (# $p < 0.05$, ****, #### $p < 0.0001$). The green is a live cell. The red is a dead cell. The blue is DAPI, n = 6.

HepG2 cells + ECs   HepG2 droplets + ECs - 1 lines   HepG2 droplets + ECs - 4 lines

Day 1

Day 3

100 µm
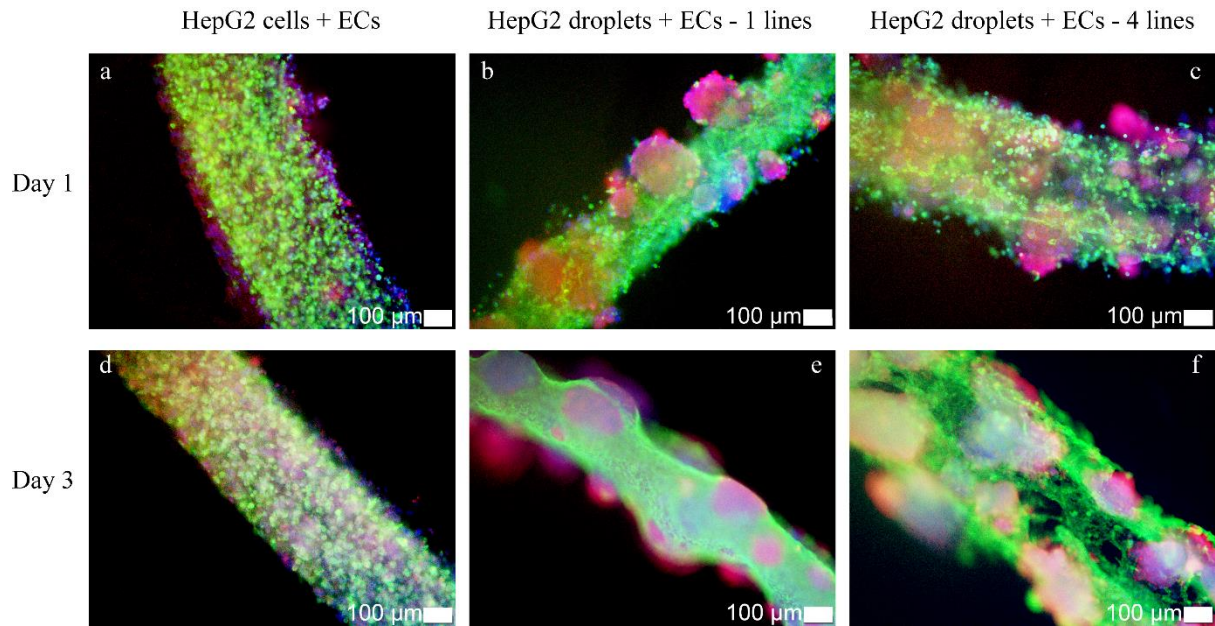
Figure 35. The immunofluorescent staining image of the fabricated scaffolds. (a - c) The images of HepG2 cells and HUVECs group; one line region of Hep2 aggregates and HUVECs group; four-line region of Hep2 aggregates and HUVECs group, respectively at day 1. (d - f) The images of HepG2 cells and HUVECs group; one line region of Hep2 aggregates and HUVECs group; four-line region of Hep2 aggregates and HUVECs group, respectively at day 3. The green is CD31. The red is albumin. The blue is DAPI.
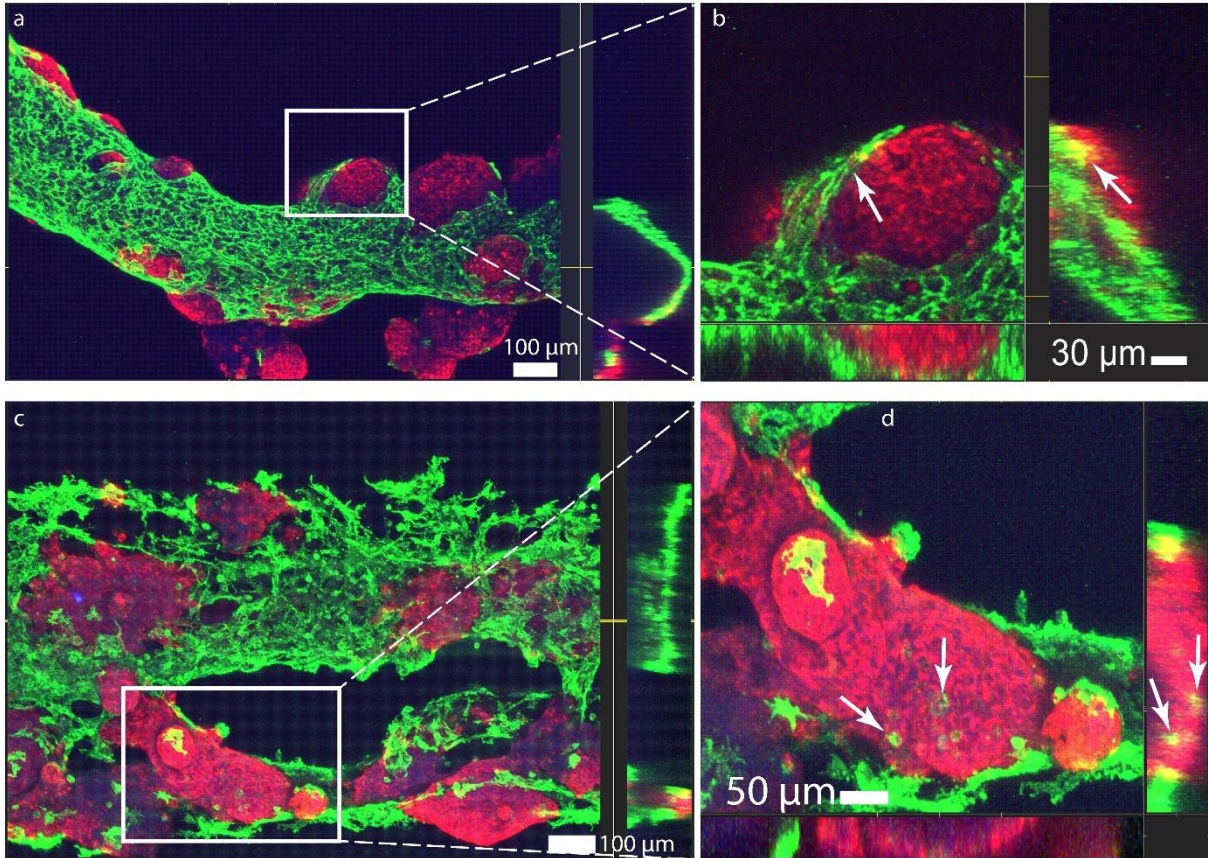
Figure 36. The confocal immunofluorescent staining image of the artificial liver scaffold. The hollow channel in one line region (a) and the four-line region (b) after 3 days culturing. The green is CD31. White arrows indicate the HUVECs spread into the HepG2 aggregate. The red is albumin. The blue is DAPI.

3.4.4 HepG2 aggregates with vascularized networks enhanced liver-specific functional expression of scaffolds

The liver provides various essential functions, including protein synthesis and metabolism. The secretion of albumin, which is a representative protein synthesized by hepatocytes and the synthesis of urea, which is indicative of the metabolism from hepatocytes are helpful markers of typical liver function [91, 92].

The culture medium was harvested at 1 day after scaffold fabrication (pre-culture), day 3 and day 7 during culturing with alginate lyase for analysis (Fig. 36). For albumin secretion, in the group of only HepG2 cells (group 1) reached 4.94 ± 0.4 µg/mL, when the group with HepG2 aggregates and HUVECs (group 2) reached 6.61 ± 0.3 µg/mL after 7 days of culturing.

The urea concentration changed over time and varied among the two groups. On day 7, in group 1 the amount of synthesized urea increased gradually from 2.50 ± 0.2 µg/mL to 6.25 ± 1.0 µg/mL, but remained lower than that of group 3 with 10.96 ± 1.4 µg/mL (1.7-fold time). These results showed that HepG2 aggregates with vascularized networks in the artificial liver scaffolds can express higher liver cell activity.
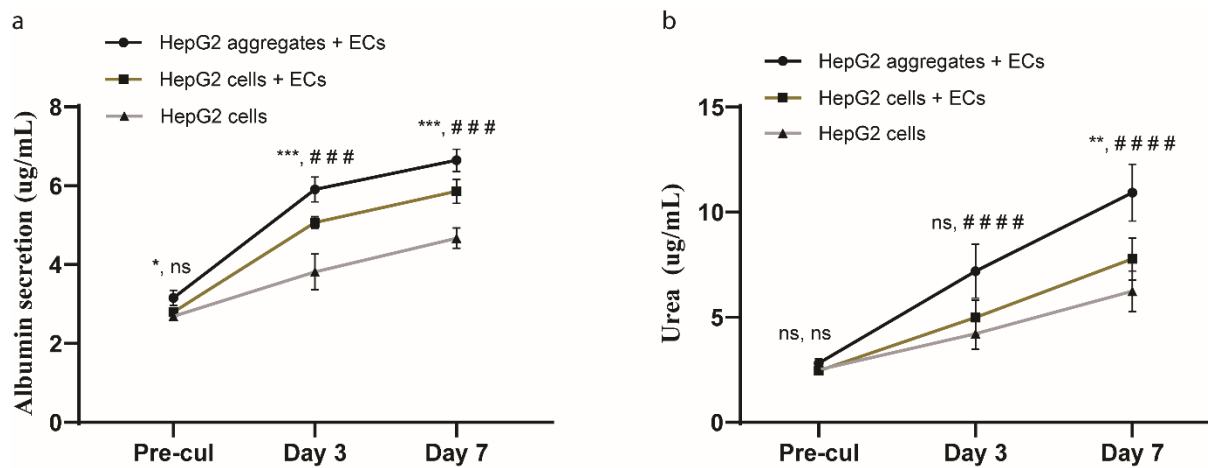
Figure 37. Time courses of albumin secretion (a) and urea synthesis (b) as markers of liver activity from HepG2 cells. Experiments were performed with n = 6 and the values are reported as means ± SD (* $p < 0.05$; ** $p < 0.01$; ***, ### $p < 0.001$; ****, #### $p < 0.0001$).

Chapter 4: Conclusion

The dissertation achieved remarkable results and the objectives of this research were demonstrated. We developed a vasculature network using the combination of acoustic standing wave forces and multi-hydrogel extrusion. This experimental model can be used to rapidly extrusion the endothelial cell networks inside the hydrogel. The amplifier circuit has no significant impact on the cell survival and the cell viability was reported to be 90% after 12 hours of scaffold fabrication and culturing. Furthermore, the selected cell density (8×10^6) approximated the report by other authors for tubular formation and may overcome one main disadvantage of scaffold-based tissue engineering is low seeding density, as well. The fabricated structures were cultured for assessing cell proliferation, cell-cell intercellular communication, and vascular network formation with the distance between vessels being almost less than 100 µm. The patterned endothelial cells matured as functional vessel networks such as angiogenesis, perfusability, and implantability.

In animal studies, the process of subcutaneous implantation revealed fascinating insights into tissue integration and vascularization. Following the subcutaneous implantation of the scaffold, within a period of three to fourteen days, researchers observed a significant interaction between the host's preexisting blood vessels and the preformed vessels within the scaffold. This interaction was marked by the host's blood vessels sprouting towards and integrating with the preformed vessels of the scaffold over time, a process that was meticulously visualized through advanced imaging techniques. Interestingly, the majority of the microvessels within the implant scaffolds demonstrated a remarkable maturation process. Initially presenting as empty tubular structures, these microvessels gradually evolved into functional blood-carrying vessels. This capability is crucial for the scaffold's successful integration and functionality within the host tissue. These findings collectively underscore the successful incorporation of the scaffold into the host tissue. The

울산대학교
UNIVERSITY OF ULSAN

ability of the scaffold to not only support the formation of functional blood vessels but also to enhance the ECM composition is a promising indicator of its potential for therapeutic applications. The improved vascularization ensures an adequate blood supply, which is vital for the delivery of nutrients and oxygen to the implanted tissue, while the enriched ECM provides the necessary support for cellular activities and tissue maintenance. The observed vascularization and ECM enhancement following the implantation of the scaffold in animal models demonstrate its potential effectiveness in tissue engineering applications. These results pave the way for further research and development of scaffold-based therapies for tissue repair and regeneration, offering hope for improved outcomes in clinical settings.

In addition, this innovative approach was also applied to the fabrication of artificial liver scaffolds, which serve as the basic structural units of liver tissue. The methodology involved patterning endothelial cells into branched structures, which were then strategically surrounded by aggregates of HepG2 cells, a line of human liver cancer cells often used in research as a model for hepatocytes, the main functional cells of the liver. The co-culture of endothelial cells and HepG2 cells resulted in enhanced vascularization within the artificial liver scaffold. This improved vascularization is crucial for the functionality of the scaffold, as it ensures an adequate supply of oxygen and nutrients while facilitating the removal of metabolic waste products. Moreover, the presence of a robust vascular network supports the proliferation and survival of hepatocytes, thereby enhancing overall liver function. The enhanced liver function observed in these studies is indicative of the scaffold's potential to replicate the complex physiological activities of natural liver tissue. Functions such as albumin production, urea synthesis, and detoxification processes are essential for maintaining metabolic homeostasis, and their enhancement in the artificial liver scaffold suggests a promising route for therapeutic applications. Consequently,

this approach holds the potential to pave the way for the generation of fully vascularized artificial livers. Such advancements are not merely academic; they have profound implications for regenerative medicine and liver transplantation. The ability to create a fully functional, vascularized artificial liver could address the critical shortage of donor organs and provide new treatment options for patients with liver diseases.

References

[1]   America. D L 2021 Organ, Eye and Tissue Donation Statistics.

[2]   Kang B, Shin J, Park H-J, Rhyou C, Kang D, Lee S-J, Yoon Y-s, Cho S-W and Lee H 2018 High-resolution acoustophoretic 3D cell patterning to construct functional collateral cylindroids for ischemia therapy *Nature Communications* **9** 5402

[3]   Hartung G, Badr S, Moeini M, Lesage F, Kleinfeld D, Alaraj A and Linninger A 2021 Voxelized simulation of cerebral oxygen perfusion elucidates hypoxia in aged mouse cortex *PLOS Computational Biology* **17** e1008584

[4]   Cui H, Zhu W, Huang Y, Liu C, Yu Z X, Nowicki M, Miao S, Cheng Y, Zhou X, Lee S J, Zhou Y, Wang S, Mohiuddin M, Horvath K and Zhang L G 2019 In vitro and in vivo evaluation of 3D bioprinted small-diameter vasculature with smooth muscle and endothelium *Biofabrication* **12** 015004

[5]   Tiruvannamalai Annamalai R, Rioja A Y, Putnam A J and Stegemann J P 2016 Vascular Network Formation by Human Microvascular Endothelial Cells in Modular Fibrin Microtissues *ACS Biomaterials Science & Engineering* **2** 1914-25

[6]   Rouwkema J and Khademhosseini A 2016 Vascularization and Angiogenesis in Tissue Engineering: Beyond Creating Static Networks *Trends in Biotechnology* **34** 733-45

[7]   Asakawa N, Shimizu T, Tsuda Y, Sekiya S, Sasagawa T, Yamato M, Fukai F and Okano T 2010 Pre-vascularization of in vitro three-dimensional tissues created by cell sheet engineering *Biomaterials* **31** 3903-9

[8]   Grainger S J and Putnam A J 2011 Assessing the Permeability of Engineered Capillary Networks in a 3D Culture *PLOS ONE* **6** e22086

[9]   Dizeux A 2015 Ultrasound characterization of tumor angiogenesis, stiffness and microstructure under conventional and innovative therapies

[10]   Jouda H, Murillo L and Wang T 2022 Current Progress in Vascular Engineering and Its Clinical Applications *Cells* **11** 493

[11]   J. Gordon Betts K A Y, James A. Wise, Eddie Johnson, Brandon Poe, Dean H. Kruse, Oksana Korol, Jody E. Johnson, Mark Womble, Peter DeSaix Apr 25, 2013 *Anatomy and Physiology*: OpenStax)

[12]   Inglebert M 2020 Blood flow in biomimetics microchanels.

[13]   Marei I, Abu Samaan T, Al-Quradaghi M, Farah A, Mahmud S H, Ding H and Triggle C 2022 3D Tissue-Engineered Vascular Drug Screening Platforms: Promise and Considerations *Frontiers in Cardiovascular Medicine* **9**

[14] Au - Davis J, Au - Crampton S P and Au - Hughes C C W 2007 Isolation of Human Umbilical Vein Endothelial Cells (HUVEC) *JoVE* e183

[15] Hauser S, Jung F and Pietzsch J 2017 Human Endothelial Cell Models in Biomaterial Research *Trends in Biotechnology* **35** 265-77

[16] Kocherova I, Bryja A, Mozdziak P, Angelova Volponi A, Dyszkiewicz-Konwińska M, Piotrowska-Kempisty H, Antosik P, Bukowska D, Bruska M, Iżycki D, Zabel M, Nowicki M and Kempisty B 2019 Human Umbilical Vein Endothelial Cells (HUVECs) Co-Culture with Osteogenic Cells: From Molecular Communication to Engineering Prevascularised Bone Grafts *Journal of Clinical Medicine* **8** 1602

[17] Song J, Miermont A, Lim C T and Kamm R D 2018 A 3D microvascular network model to study the impact of hypoxia on the extravasation potential of breast cell lines *Scientific Reports* **8** 17949

[18] Park Y K, Tu T-Y, Lim S H, Clement I J M, Yang S Y and Kamm R D 2014 In Vitro Microvessel Growth and Remodeling within a Three-Dimensional Microfluidic Environment *Cellular and Molecular Bioengineering* **7** 15-25

[19] Vailhé B, Vittet D and Feige J-J 2001 In Vitro Models of Vasculogenesis and Angiogenesis *Laboratory Investigation* **81** 439-52

[20] Lesman A, Rosenfeld D, Landau S and Levenberg S 2016 Mechanical regulation of vascular network formation in engineered matrices *Advanced Drug Delivery Reviews* **96** 176-82

[21] Pavlovic M 2014 *Bioengineering: A Conceptual Approach*: Springer International Publishing)

[22] Safina I and Embree M C 2022 Biomaterials for recruiting and activating endogenous stem cells in situ tissue regeneration *Acta Biomaterialia* **143** 26-38

[23] Mozafari M and Chauhan N P S 2023 *Handbook of Polymers in Medicine*: Elsevier Science)

[24] Liu S, Yu J-M, Gan Y-C, Qiu X-Z, Gao Z-C, Wang H, Chen S-X, Xiong Y, Liu G-H, Lin S-E, McCarthy A, John J V, Wei D-X and Hou H-H 2023 Biomimetic natural biomaterials for tissue engineering and regenerative medicine: new biosynthesis methods, recent advances, and emerging applications *Military Medical Research* **10** 16

[25] Eldeeb A E, Salah S and Elkasabgy N A 2022 Biomaterials for Tissue Engineering Applications and Current Updates in the Field: A Comprehensive Review *AAPS PharmSciTech* **23** 267

[26] Porzionato A, Sfriso M M, Macchi V, Rambaldo A, Lago G, Lancerotto L, Vindigni V and De Caro R 2013 Decellularized omentum as novel biologic scaffold for reconstructive surgery and regenerative medicine *European Journal of Histochemistry* **57** e4

울산대학교
UNIVERSITY OF ULSAN

[27] Giobbe G G, Crowley C, Luni C, Campinoti S, Khedr M, Kretzschmar K, De Santis M M, Zambaiti E, Michielin F, Meran L, Hu Q, van Son G, Urbani L, Manfredi A, Giomo M, Eaton S, Cacchiarelli D, Li V S W, Clevers H, Bonfanti P, Elvassore N and De Coppi P 2019 Extracellular matrix hydrogel derived from decellularized tissues enables endodermal organoid culture *Nature Communications* **10** 5658

[28] Aamodt J M and Grainger D W 2016 Extracellular matrix-based biomaterial scaffolds and the host response *Biomaterials* **86** 68-82

[29] Duong V T, Nguyen C T, Phan H L, Le V P, Dang T T, Choi C, Seo J, Cha C, Back S H and Koo K-i 2023 Double-layered blood vessels over 3 mm in diameter extruded by the inverse-gravity technique *Biofabrication* **15** 045022

[30] Kinsler L E, Frey A R, Coppens A B and Sanders J V 2000 *Fundamentals of acoustics*: John wiley & sons)

[31] Shi J, Ahmed D, Mao X, Lin S-C S, Lawit A and Huang T J 2009 Acoustic tweezers: patterning cells and microparticles using standing surface acoustic waves (SSAW) *Lab on a Chip* **9** 2890-5

[32] Shi J, Mao X, Ahmed D, Colletti A and Huang T J 2008 Focusing microparticles in a microfluidic channel with standing surface acoustic waves (SSAW) *Lab on a Chip* **8** 221-3

[33] Garvin K A, Dalecki D and Hocking D C 2011 Vascularization of Three-Dimensional Collagen Hydrogels Using Ultrasound Standing Wave Fields *Ultrasound in Medicine & Biology* **37** 1853-64

[34] Comeau E S, Hocking D C and Dalecki D 2017 Ultrasound patterning technologies for studying vascular morphogenesis in 3D *Journal of Cell Science* **130** 232-42

[35] Trujillo F J, Juliano P, Barbosa-Cánovas G and Knoerzer K 2014 Separation of suspensions and emulsions via ultrasonic standing waves – A review *Ultrasonics Sonochemistry* **21** 2151-64

[36] Hill M and Harris N R 1970 pp 357-92

[37] Koo K-i, Lenshof A, Huong L T and Laurell T 2021 Acoustic Cell Patterning in Hydrogel for Three-Dimensional Cell Network Formation *Micromachines* **12** 3

[38] Red-Horse K and Siekmann A F 2019 Veins and Arteries Build Hierarchical Branching Patterns Differently: Bottom-Up versus Top-Down *Bioessays* **41** e1800198

[39] Laschke M W, Mussawy H, Schuler S, Kazakov A, Rücker M, Eglin D, Alini M and Menger M D 2010 Short-Term Cultivation of In Situ Prevascularized Tissue Constructs Accelerates Inosculation of Their Preformed Microvascular Networks After Implantation into the Host Tissue *Tissue Engineering Part A* **17** 841-53

울산대학교
UNIVERSITY OF ULSAN

[40] Santos M I and Reis R L 2010 Vascularization in bone tissue engineering: physiology, current strategies, major hurdles and future challenges *Macromol Biosci* **10** 12-27

[41] Pries A R and Secomb T W 2014 Making Microvascular Networks Work: Angiogenesis, Remodeling, and Pruning *Physiology* **29** 446-55

[42] Pill K, Melke J, Mühleder S, Pultar M, Rohringer S, Priglinger E, Redl H R, Hofmann S and Holnthoner W 2018 Microvascular Networks From Endothelial Cells and Mesenchymal Stromal Cells From Adipose Tissue and Bone Marrow: A Comparison *Frontiers in Bioengineering and Biotechnology* **6**

[43] Park J Y, Ryu H, Lee B, Ha D H, Ahn M, Kim S, Kim J Y, Jeon N L and Cho D W 2018 Development of a functional airway-on-a-chip by 3D cell printing *Biofabrication* **11** 015002

[44] Nguyen C T, Duong V T, Hwang C H and Koo K I 2022 Angiogenesis in Free-Standing Two-Vasculature-Embedded Scaffold Extruded by Two-Core Laminar Flow Device *Int J Bioprint* **8** 557

[45] Duong V T, Dang T T, Kim J P, Kim K, Ko H, Hwang C H and Koo K I 2019 Twelve-day medium pumping into tubular cell-laden scaffold using a lab-made PDMS connector *Eur Cell Mater* **38** 1-13

[46] Zhu W, Qu X, Zhu J, Ma X, Patel S, Liu J, Wang P, Lai C S E, Gou M, Xu Y, Zhang K and Chen S 2017 Direct 3D bioprinting of prevascularized tissue constructs with complex microarchitecture *Biomaterials* **124** 106-15

[47] Andrique L, Recher G, Alessandri K, Pujol N, Feyeux M, Bon P, Cognet L, Nassoy P and Bikfalvi A 2019 A model of guided cell self-organization for rapid and spontaneous formation of functional vessels *Science Advances* **5** eaau6562

[48] Serpooshan V, Chen P, Wu H, Lee S, Sharma A, Hu D A, Venkatraman S, Ganesan A V, Usta O B, Yarmush M, Yang F, Wu J C, Demirci U and Wu S M 2017 Bioacoustic-enabled patterning of human iPSC-derived cardiomyocytes into 3D cardiac tissue *Biomaterials* **131** 47-57

[49] Ohlsson P, Petersson K, Augustsson P and Laurell T 2018 Acoustic impedance matched buffers enable separation of bacteria from blood cells at high cell concentrations *Scientific Reports* **8** 9156

[50] Petersson F, Åberg L, Swärd-Nilsson A-M and Laurell T 2007 Free Flow Acoustophoresis: Microfluidic-Based Mode of Particle and Cell Separation *Analytical Chemistry* **79** 5117-23

[51] Urbansky A, Ohlsson P, Lenshof A, Garofalo F, Scheding S and Laurell T 2017 Rapid and effective enrichment of mononuclear cells from blood using acoustophoresis *Scientific Reports* **7** 17161

[52] Magnusson C, Augustsson P, Lenshof A, Ceder Y, Laurell T and Lilja H 2017 Clinical-Scale Cell-Surface-Marker Independent Acoustic

Microfluidic Enrichment of Tumor Cells from Blood *Analytical Chemistry* **89** 11954-61

[53] Jakobsson O, Oh S S, Antfolk M, Eisenstein M, Laurell T and Soh H T 2015 Thousand-Fold Volumetric Concentration of Live Cells with a Recirculating Acoustofluidic Device *Analytical Chemistry* **87** 8497-502

[54] Lenshof A, Ahmad-Tajudin A, Järås K, Swärd-Nilsson A M, Aberg L, Marko-Varga G, Malm J, Lilja H and Laurell T 2009 Acoustic whole blood plasmapheresis chip for prostate specific antigen microarray diagnostics *Anal Chem* **81** 6030-7

[55] Parasuraman S, Raveendran R and Kesavan R 2010 Blood sample collection in small laboratory animals *J Pharmacol Pharmacother* **1** 87-93

[56] Duong V T, Dang T T, Hwang C H, Back S H and Koo K-i 2020 Coaxial printing of double-layered and free-standing blood vessel analogues without ultraviolet illumination for high-volume vascularised tissue *Biofabrication* **12** 045033

[57] Jeon O, Bouhadir K H, Mansour J M and Alsberg E 2009 Photocrosslinked alginate hydrogels with tunable biodegradation rates and mechanical properties *Biomaterials* **30** 2724-34

[58] Tahir I and Floreani R 2022 Dual-Crosslinked Alginate-Based Hydrogels with Tunable Mechanical Properties for Cultured Meat *Foods* **11** 2829

[59] Nwe N, Furuike T and Tamura H 2010 Selection of a biopolymer based on attachment, morphology and proliferation of fibroblast NIH/3T3 cells for the development of a biodegradable tissue regeneration template: Alginate, bacterial cellulose and gelatin *Process Biochemistry* **45** 457-66

[60] Abaci A and Guvendiren M 2020 Designing Decellularized Extracellular Matrix-Based Bioinks for 3D Bioprinting *Adv Healthc Mater* **9** e2000734

[61] Spang M T and Christman K L 2018 Extracellular matrix hydrogel therapies: In vivo applications and development *Acta Biomater* **68** 1-14

[62] Kim B S, Das S, Jang J and Cho D-W 2020 Decellularized Extracellular Matrix-based Bioinks for Engineering Tissue- and Organ-specific Microenvironments *Chemical Reviews* **120** 10608-61

[63] Huang C C 2021 Characteristics and Preparation of Designed Alginate-Based Composite Scaffold Membranes with Decellularized Fibrous Micro-Scaffold Structures from Porcine Skin *Polymers (Basel)* **13**

[64] DeCicco-Skinner K L, Henry G H, Cataisson C, Tabib T, Gwilliam J C, Watson N J, Bullwinkle E M, Falkenburg L, O'Neill R C, Morin A and Wiest J S 2014 Endothelial cell tube formation assay for the in vitro study of angiogenesis *J Vis Exp* e51312-e

[65] Petta D, Basoli V, Pellicciotta D, Tognato R, Barcik J, Arrigoni C, Bella E D, Armiento A R, Candrian C, Richards R G, Alini M, Moretti M, Eglin D and Serra T 2021 Sound-induced morphogenesis of multicellular

systems for rapid orchestration of vascular networks *Biofabrication* **13** 015004

[66] Hasday J D, Bannerman D, Sakarya S, Cross A S, Singh I S, Howard D, Drysdale B-E and Goldblum S E 2001 Exposure to febrile temperature modifies endothelial cell response to tumor necrosis factor-α *Journal of Applied Physiology* **90** 90-8

[67] Ashton R S, Banerjee A, Punyani S, Schaffer D V and Kane R S 2007 Scaffolds based on degradable alginate hydrogels and poly(lactide-co-glycolide) microspheres for stem cell culture *Biomaterials* **28** 5518-25

[68] Andersen T, Auk-Emblem P and Dornish M 2015 3D Cell Culture in Alginate Hydrogels *Microarrays (Basel)* **4** 133-61

[69] Kim H S, Lee C-G and Lee E Y 2011 Alginate lyase: Structure, property, and application *Biotechnology and Bioprocess Engineering* **16** 843

[70] Martin M, Veloso A, Wu J, Katrukha E A and Akhmanova A 2018 Control of endothelial cell polarity and sprouting angiogenesis by non-centrosomal microtubules *Elife* **7** e33864

[71] Haskard D O, Boyle J J, Evans P C, Mason J C and Randi A M 2013 Cytoprotective Signaling and Gene Expression in Endothelial Cells and Macrophages—Lessons for Atherosclerosis *Microcirculation* **20** 203-16

[72] Wallez Y and Huber P 2008 Endothelial adherens and tight junctions in vascular homeostasis, inflammation and angiogenesis *Biochimica et Biophysica Acta (BBA) - Biomembranes* **1778** 794-809

[73] Bazzoni G 2011 Pathobiology of junctional adhesion molecules *Antioxid Redox Signal* **15** 1221-34

[74] Gao G, Park J Y, Kim B S, Jang J and Cho D-W 2018 Coaxial Cell Printing of Freestanding, Perfusable, and Functional In Vitro Vascular Models for Recapitulation of Native Vascular Endothelium Pathophysiology *Advanced Healthcare Materials* **7** 1801102

[75] Grimes D R, Kannan P, Warren D R, Markelc B, Bates R, Muschel R and Partridge M 2016 Estimating oxygen distribution from vasculature in three-dimensional tumour tissue *J R Soc Interface* **13** 20160070

[76] Sosa J M, Nielsen N D, Vignes S M, Chen T G and Shevkoplyas S S 2014 The relationship between red blood cell deformability metrics and perfusion of an artificial microvascular network *Clin Hemorheol Microcirc* **57** 275-89

[77] Kim L, Toh Y-C, Voldman J and Yu H 2007 A practical guide to microfluidic perfusion culture of adherent mammalian cells *Lab on a Chip* **7** 681-94

[78] Hosseini V, Maroufi N F, Saghati S, Asadi N, Darabi M, Ahmad S N S, Hosseinkhani H and Rahbarghazi R 2019 Current progress in hepatic tissue regeneration by tissue engineering *Journal of Translational Medicine* **17** 383

[79] Mazza G, Al-Akkad W, Rombouts K and Pinzani M 2018 Liver tissue engineering: From implantable tissue to whole organ engineering *Hepatol Commun* **2** 131-41

[80] Jeon H, Kang K, Park S A, Kim W D, Paik S S, Lee S H, Jeong J and Choi D 2017 Generation of Multilayered 3D Structures of HepG2 Cells Using a Bio-printing Technique *Gut Liver* **11** 121-8

[81] Lee J S, Shin J, Park H-M, Kim Y-G, Kim B-G, Oh J-W and Cho S-W 2014 Liver Extracellular Matrix Providing Dual Functions of Two-Dimensional Substrate Coating and Three-Dimensional Injectable Hydrogel Platform for Liver Tissue Engineering *Biomacromolecules* **15** 206-18

[82] Uygun B E, Soto-Gutierrez A, Yagi H, Izamis M L, Guzzardi M A, Shulman C, Milwid J, Kobayashi N, Tilles A, Berthiaume F, Hertl M, Nahmias Y, Yarmush M L and Uygun K 2010 Organ reengineering through development of a transplantable recellularized liver graft using decellularized liver matrix *Nat Med* **16** 814-20

[83] Hirose M, Yamato M, Kwon O H, Harimoto M, Kushida A, Shimizu T, Kikuchi A and Okano T 2000 Temperature-Responsive surface for novel co-culture systems of hepatocytes with endothelial cells: 2-D patterned and double layered co-cultures *Yonsei Med J* **41** 803-13

[84] Bhandari R N, Riccalton L A, Lewis A L, Fry J R, Hammond A H, Tendler S J and Shakesheff K M 2001 Liver tissue engineering: a role for co-culture systems in modifying hepatocyte function and viability *Tissue Eng* **7** 345-57

[85] Kim K, Ohashi K, Utoh R, Kano K and Okano T 2012 Preserved liver-specific functions of hepatocytes in 3D co-culture with endothelial cell sheets *Biomaterials* **33** 1406-13

[86] Kim M, Lee J Y, Jones C N, Revzin A and Tae G 2010 Heparin-based hydrogel as a matrix for encapsulation and cultivation of primary hepatocytes *Biomaterials* **31** 3596-603

[87] Mao Q, Wang Y, Li Y, Juengpanich S, Li W, Chen M, Yin J, Fu J and Cai X 2020 Fabrication of liver microtissue with liver decellularized extracellular matrix (dECM) bioink by digital light processing (DLP) bioprinting *Materials Science and Engineering: C* **109** 110625

[88] Karthick S, Pradeep P N, Kanchana P and Sen A K 2018 Acoustic impedance-based size-independent isolation of circulating tumour cells from blood using acoustophoresis *Lab on a Chip* **18** 3802-13

[89] Wong S F, No D Y, Choi Y Y, Kim D S, Chung B G and Lee S-H 2011 Concave microwell based size-controllable hepatosphere as a three-dimensional liver tissue model *Biomaterials* **32** 8087-96

[90] Pang Y, Montagne K, Shinohara M, Komori K and Sakai Y 2012 Liver tissue engineering based on aggregate assembly: efficient formation of

endothelialized rat hepatocyte aggregates and their immobilization with biodegradable fibres* *Biofabrication* **4** 045004

[91]	Su W T, Liu Y J and Huang T Y 2016 Nanofibers promote HepG2 aggregate formation and cellular function *Genet Mol Res* **15**

[92]	Lee J W, Choi Y-J, Yong W-J, Pati F, Shim J-H, Kang K S, Kang I-H, Park J and Cho D-W 2016 Development of a 3D cell printed construct considering angiogenesis for liver tissue engineering *Biofabrication* **8** 015007

울산대학교
UNIVERSITY OF ULSAN

Appendices

Credits & Copyright Permissions

Notes on Copyright Licenses for Reproduction of Text and Figures in this Dissertation

Chapter 1:

For reproducing those figures that appeared in the following publication with credit to other sources, permission has also been sought from the respective sources.

Chapter 2

The text excerpts and the figures presented in chapter 2 are reproduced with permission from the following articles:

Huong Thi Le, Huu Lam Phan, Andreas Lenshof, Cholong Choi, Chaenyung Cha, Thomas Laurell, Kyo-in Koo, "Ultrasound standing wave spatial patterning of human umbilical vein endothelial cells for 3D micro-vascular networks formation", Biofabrication, 2023, DOI: 10.1088/1758-5090/ad03be.